

CLEAR: Coverage-based Limiting-cell Experiment Analysis for RNA-seq

Logan A Walker^{1,2}, Michael G Sovic², Chi-Ling Chiang^{2,3}, Eileen Hu^{2,3}, Jiyeon K Denninger⁴, Xi Chen², Elizabeth D Kirby⁴, John C Byrd^{2,3}, Natarajan Muthusamy^{2,3}, Ralf Bundschuh^{1,3,5,6*}, and Pearly Yan^{2,3*}

¹*Department of Physics, College of Arts and Sciences,* ²*The Ohio State University Comprehensive Cancer Center,* ³*Division of Hematology, Department of Internal Medicine, College of Medicine,* ⁴*Department of Psychology, College of Arts and Sciences,* ⁵*Department of Chemistry & Biochemistry, College of Arts and Sciences,* ⁶*Center for RNA Biology, The Ohio State University, Columbus, OH*

* To whom correspondence should be addressed. Tel: +1 614 688 3978 and +1 614 685 9164; Email: bundschuh@mps.ohio-state.edu and Pearly.Yan@osumc.edu; Mail: 460 W. 12th Ave. Room 285, Columbus, OH 43210.

ABSTRACT

Direct cDNA preamplification protocols developed for single-cell RNA-seq (scRNA-seq) have enabled transcriptome profiling of rare cells without having to pool multiple samples or to perform RNA extraction. We term this approach limiting-cell RNA-seq (lcRNA-seq). Unlike scRNA-seq, which focuses on 'cell-atlasing', lcRNA-seq focuses on identifying differentially expressed genes (DEGs) between experimental groups. This requires accounting for systems noise which can obscure biological differences. We present CLEAR, a workflow that identifies robust transcripts in lcRNA-seq data for between-group comparisons. To develop CLEAR, we compared DEGs from RNA extracted from FACS-derived CD5+ and CD5- cells from a single chronic lymphocytic leukemia patient diluted to input RNA levels of 10-, 100- and 1,000pg. Data quality at ultralow input levels are known to be noisy. When using CLEAR transcripts vs. using all available transcripts, downstream analyses reveal more shared DEGs, improved Principal Component Analysis separation of cell type, and increased similarity between results across different input RNA amounts. CLEAR was applied to two publicly available ultralow input RNA-seq data and an in-house murine neural cell lcRNA-seq dataset. CLEAR provides a novel way to visualize the public datasets while validates cell phenotype markers for astrocytes, neural stem and progenitor cells.

INTRODUCTION

Deep sequencing of transcriptomes (RNA-seq) provides important insights into biology and disease. The number of cells required to yield enough input for bulk RNA-seq is over 100s of thousands of cells. The resultant transcriptomic profile is therefore the average of cells at different transcriptomic states or even different cell types within the same tissues (e.g., infiltrating immune cells or normal cells in bulk tumor samples). With the discovery of new genes and splice junctions in the first single-cell RNA-seq (scRNA-seq) study (1), the research community started to appreciate the importance of profiling single-cell transcriptomes. Coinciding with this intense interest is the development of diverse approaches to perform single-cell RNA-seq, which have been summarized in recent reviews (2–5). Improvements in reagents and kits that enable full-length transcriptome profiling by direct global amplification at the single-cell level (such as SMART-seq (6–8), Quartz-Seq (9), the Tang et al. method (1), and other commercialized kits under development) also enable direct amplification for limiting-cell RNA-seq (lcRNA-seq), i.e., transcriptome analysis of groups of 10-100 cells.

The advantages of direct amplification are manifold. First, it opens up development and optimization in an area of an unmet need: the ability to perform differential gene expression analysis in projects that study rare cell populations. Until recently, researchers have had to resort to pooling rare cells from multiple samples to have sufficient cells to extract quantifiable amounts of total RNA for library generation. With direct cDNA preamplification, the number of cells required for successful library preparation dropped to below 100 cells, a level often achievable without having to pool cells from several samples. Also, as quantification of input RNA amounts below 250-pg total RNA is very challenging, direct extraction and amplification of RNA at the cell enrichment step (e.g., fluorescence activated cell sorted (FACS) or laser capture) allows standardization of input by cell counts rather than input mass. Second, direct amplification reduces many sources of RNA degradation that can stymie RNA-seq of low cell

numbers. Conditions such as sample storage and cell type enrichment prior to RNA extraction can significantly impact the quality of resultant RNA. When input amount is sufficiently high, the effect of RNA degradation may not be apparent. However, at RNA levels necessitated by rare/limiting cells, the systems noise associated with degradation products can be rather high and affect the outcomes of between-group comparisons. The direct amplification process removes the need for RNA extraction and therefore degradation associated with this step, which can be significant. Third, direct amplification of enriched cells deposited into strip tubes or well-plates allows integration of automation steps using nanoliter microfluidics devices to deliver/mix reagents and templates quickly. This further preserves RNA integrity. Additional benefits of using a semi-automated approach include increase in sample throughput, as well as decrease in processing errors, transfer loss, and personnel cost.

Although reagents and nanoliter microfluidics devices are available for efficient and robust lcrRNA-seq library preparation, a computation workflow that accounts for systems noise associated with global preamplification, especially for data derived from samples that experienced degradation as a result of sample/cell preparation is lacking. Current publications on ultralow input RNA-seq data fall into two categories: cell-pool samples as part of studies developing or comparing scRNA-seq methodologies (6, 10–12) and ultralow amounts of extracted RNA as input for RNA-seq library preparation (13–15). There exist methods and tools for bulk RNA-seq data and scRNA-seq data as each sequencing approach is designed to answer a specific but different research question. The goal of bulk RNA-seq is to identify differences in transcriptomic profiles between treatment groups whereas the goal of scRNA-seq is to characterize cell subpopulations in tissues or bulk cells. In this regard, the aim of lcrRNA-seq experiments is like that of bulk RNA-seq experiments whereas their data quality (e.g., prevalence of zero count genes, also known as dropout rate (10, 16, 17)) is similar to that of scRNA-seq. Therefore, statistical methods often used for between-group comparisons in bulk RNA-seq studies, such as the negative binomial distribution-based test in DESeq2 (18), should not be used for lcrRNA-seq data without appropriate modifications because they are known to be susceptible to zero-count artifacts associated with lcr/scRNA-seq. On the other hand, there are a myriad of tools (19–28) for analyzing scRNA-seq data. These tools are tuned to work with high variabilities such as true biological variations in small cell populations or in single cells as well as technical variabilities due to the global preamplification step. However, in order to overcome the noise resulting from global preamplification, scRNA-seq analysis methods rely heavily on a large number of single cells being sequenced. The number of replicates in these experimental designs is much larger than available in typical between-group lcrRNA-seq experiments.

Here, we describe CLEAR, a computational preprocessing approach for optimizing counts matrices utilized in between-group comparisons of globally preamplified lcrRNA-seq experiments. In the absence of large numbers of replicates, our approach focuses on identifying which transcripts are robustly quantified rather than utilizing signal from every transcript in the samples. It explicitly uses the noise pattern of each sample within each pair of comparison to identify all possible 'reliably quantifiable' transcripts ensuring maximum information yield given the amount of noise present in that sample. CLEAR transcripts common to replicates across two comparison groups will be used for downstream analyses. On a data set from libraries generated with the same RNA at different dilutions representative of typical lcrRNA-seq experiments, we show that our approach greatly improves similarity between results from three different input RNA levels. In two publicly available datasets, we demonstrate that the numbers and the dispersion patterns of CLEAR transcripts yield a novel way to evaluations of library qualities. In an in-house murine neural cell lcrRNA-seq study, utilizing CLEAR transcripts significantly improve cell type separations by Principal Component Analysis (PCA) and validations of cell phenotype markers.

MATERIALS AND METHODS

CLL Patient Sample Acquisition

A chronic lymphocytic leukemia (CLL) patient sample was obtained from the Leukemia Tissue Bank (LTB), a shared resource of the NCI-funded OSU Comprehensive Cancer Center. The sample was obtained following written informed consent in accordance with the Declaration of Helsinki and under a protocol reviewed and approved by the Institutional Review Board of the Ohio State University. The patient had CLL as defined by the IWCLL 2008 criteria. The patient's white blood cells were isolated by Ficoll density gradient centrifugation (Ficoll-Paque Plus, Amersham Biosciences, Little Chalfont, UK) and

samples were banked at -180°C in liquid nitrogen. Frozen cells were thawed and washed with RPMI 1640 media (Gibco, Life Technologies, Grand Island, NY, USA) and resuspended at 5×10^6 cells/mL in complete medium containing 10% fetal bovine serum (FBS) (Sigma, St Louis, MO, USA), 2 mM L-glutamine, penicillin (100U/mL), and streptomycin (100 $\mu\text{g}/\text{mL}$) (Gibco).

Animals for neural Cell Type Analysis
All procedures involving animals were approved by the Ohio State Institutional Animal Care and Use Committee in accordance with institutional and national guidelines. Nestin-GFP mice were provided by Grigori Enikolopov at Cold Spring Harbor Laboratory. All mice were housed in a 12-hour light-dark cycle with food and water ad libitum.

For isolation of the dentate gyrus (DG), adult mice (6-9 wk old) were anesthetized with an intraperitoneal injection of ketamine (87.5 mg/kg) and xylazine (12.5 mg/kg) before perfusion with PBS. Following perfusion, the brain was removed and placed in cold Neurobasal A medium (Gibco 10-888-022) on ice. After bisecting the brain along the midsagittal line, the cerebellum and diencephalic structures were removed to expose the hippocampus. Under a dissection microscope (Zeiss), the DG was excised using a beveled syringe needle and placed in ice cold PBS without calcium or magnesium (Gibco 10-010-049). DGs from mice were first mechanically dissociated with sterile scalpel blades and then enzymatically dissociated with a pre-warmed papain (Roche 10108014001)/dispase (Stem Cell Technologies 07913)/DNase (Stem Cell Technologies NC9007308) (PDD) cocktail at 37°C for 20 min. Afterwards, the tissue was again mechanically disrupted by trituration for 1 min. Dissociated cells were collected by centrifugation at 500g for 5 min.

Fluorescence activated cell sorting (FACS)

For the human sample all cells were stained and sorted by FACS Aria (BD Biosciences, San Jose, CA, USA). Live CLL B cells (CD5+CD19+) and normal B cells (CD5-CD19+) were sorted from the patient sample. Briefly, cells for FACS were resuspended in PBS without calcium/magnesium and filtered through a $35\mu\text{m}$ nylon filter and then stained for PE-conjugated CD45 (HI30), PerCp Cy-5.5-conjugated CD19 (HIB19), and Alexa Fluor 700-conjugated CD3 (UCHT1) monoclonal antibodies. Nonviable cells were excluded by the LIVE/DEAD Fixable Near-IR Dead Cell Stain Kit (Life Technologies, Carlsbad, CA, USA). Appropriate fluorescence minus one controls were used to determine nonspecific background staining. Single-cell gates were used to exclude the possibility of doublet cells. The FACS parameter diagrams for this process are available in Figure S1.

For the Nestin-GFP mouse samples, cells were resuspended in PBS without calcium/magnesium and filtered through a $35\mu\text{m}$ nylon filter before staining with the following antibodies: O4-APC (1:100, R&D FAB1326A), O1-eFluor660 (1:100, Thermo Fisher/eBioscience, Pittsburgh, PA, 5065082), GLAST-PE (1:50, Miltenyi Biotec, Bergisch Gladbach, Germany, 130-098-804), CD45-APC (1:100, BD Biosciences, Franklin Lakes, NJ, 561018), CD31-APC (1:100, BD Biosciences, Franklin Lakes, NJ, 561814). Cells were incubated with antibodies on ice for 30 minutes. During the last 10 minutes of staining, Hoechst dye (1:10,000, Thermo Fisher, Pittsburgh, PA, 33342) was added for live/dead discrimination. All cells were washed twice following staining and immediately sorted as stem, progenitor, or astrocyte populations based on fluorescent markers with the FACS Aria III (BD Biosciences, Franklin Lakes, NJ). CD31, CD45, O1, and O4 negative live cells were designated as stem cells if double positive for GLAST and GFP, progenitors if only GFP positive, and astrocytes if only GLAST positive. For cells in the limited cell number study, 50 cells were sorted into 96 well format plate for downstream lcrRNA-seq library generation.

Total RNA Extraction

Total RNA extraction was performed using Trizol reagent (Invitrogen, Carlsbad, CA). Briefly, approximately two million FACS-derived CD5+ and CD5- cells were separately sorted into 1.7 ml microcentrifuge tubes. Excess buffer was removed by centrifugation. Trizol reagent was added to cell pellets and the extraction protocol recommended by Invitrogen was followed. Total RNA was precipitated with 10 μg glycogen (Qiagen, Hilden, Germany). The quality of the total RNA was assessed with the Agilent 2100 Bioanalyzer (Agilent, Inc., Santa Clara, CA) using total RNA Pico chip.

Library Generation and Sample Sequencing

Total CD5+ and CD5- RNA quantified using the Invitrogen Qubit RNA HS Assay kit (Invitrogen, Carlsbad, CA) was serially diluted to masses characteristic of single- and low cell number RNA-Seq (10-, 100-, and 1000-pg). The Clontech SMARTer v4 kit (Takara Bio USA, Inc., Mountain View, CA) was used for global preamplification of these serially diluted samples in triplicate and also for direct global preamplification in FACS-derived murine DG cell types prior to library generation in quadruplicates with the Nextera XT DNA Library Prep kit (Illumina, Inc., San Diego, CA). Samples were sequenced to a depth of 15 - 20 million 2x150 bp clusters on the Illumina HiSeq 4000 platform (Illumina, Inc., San Diego, CA).

Publicly Available Data Retrieval

Additional published data was retrieved in FASTQ format from the following accession numbers: ArrayExpress E-MTAB-2600 (29) (mouse embryonic stem cells from 2i and alternative 2i media) and GSE50856 (14) (SMART-seq samples) for validation of CLEAR.

Data Preprocessing, Alignment, and Quantification

Individual FASTQ files were trimmed for adapter sequences and filtered for a minimum quality score of Q20 using AdapterRemoval v2.2.0 (30). Preliminary alignment using HISAT2 v2.0.6 (31) was performed to a composite reference of rRNA, mtDNA, and PhiX bacteriophage sequences obtained from NCBI RefSeq (32). Reads aligning to these references were excluded in downstream analyses. Primary alignment was performed against the human genome reference GRCh38p7 or mouse genome reference GRCm38p4 using HISAT2. Gene expression values for genes described by the GENCODE (33, 34) Gene Transfer Format (GTF) release 25 (human) or release M14 (mouse) were quantified using the featureCounts tool of the Subread package v1.5.1 (35) in unstranded mode.

Quality Control

Quality control was performed using a modification of our custom workflow QuaCRS (36). In brief, aligned read quality was verified using RNA-SeQC (37) and RSeQC (38). Parameters evaluated included the exonic rate (the percentage of reads aligning to exons), the intronic rate (the percentage of reads aligning to introns), and the duplication rate (the percentage of reads that were identified as PCR duplicates).

Coverage Profiling

Coverage depths across the aligned reference were calculated with a per-base resolution using the 'genomecov' utility of Bedtools v2.27.0 (39) in BedGraph format. It is imperative to utilize 'split output' mode to reduce the size of the output BedGraph files. These files are used as input into CLEAR.

Calculation of Transcript μ_i

For each primary transcript annotated in the GENCODE GTF file, CLEAR calculates the transcript's μ_i parameter. This quantifies the distribution of the positional mean of the read distribution along that transcript between the 5' ($\mu_i = -1$) and the 3' ($\mu_i = +1$) ends (Equation 1):

$$\mu_i = \frac{2}{L_{\text{transcript}}} \left(\frac{\sum_{k=0}^{L_{\text{transcript}}-1} (k \cdot d_k)}{\sum_{k=0}^{L_{\text{transcript}}-1} (d_k)} \right) - 1 \quad (1)$$

where $L_{\text{transcript}}$ is the length of a given transcript, and d_k is the coverage of exomic locus k zero indexed and starting at the transcription start site.

Determination of Analysis-Ready CLEAR Transcripts

All transcripts quantified by featureCounts are sorted by overall expression. Histograms, of 250 transcripts each, are collected and fit, using the Python Imfit package, to a double-gaussian model as described by Equation 2:

$$A \cdot \left(e^{-\frac{(\mu_i - t)^2}{2\sigma^2}} + e^{-\frac{(\mu_i + t)^2}{2\sigma^2}} \right) \quad (2)$$

where A is an arbitrary normalization parameter, σ is the standard deviation and t is the displacement between the Gaussian peaks. The value of μ_i is discretized into bins to allow fitting to a histogram of all values of μ_i . These windows are advanced in units of 10 transcripts, to reduce computational intensity. Once a window is found which reaches a t value of 0.5, the software selects transcripts with a higher expression than that window to be exported for analysis. For multiple-sample comparisons, transcripts were overlapped and only transcripts that CLEAR identifies in all samples were included for downstream analysis.

CLEAR Visualizations

A core component to the quality control of the CLEAR selection process is the visualization of μ_i to confirm that the characteristic bifurcation is observed. Violin plots were produced using code included with CLEAR which implements the matplotlib package in Python. Examples of this can be seen in Figures 2d, 4a, and 4c.

DEG Comparisons

Differentially expressed genes were called using DESeq2 (18) run on counts tables generated with featureCounts as described above. In all summarization figures, a false discovery rate (FDR) q-value of <0.05 was used as an inclusion criterion for DEGs.

Principal Component Analysis

Principal component analysis (PCA) was utilized to visualize differences between samples. All PCA plots were generated from counts tables that were size-normalized and r-log transformed after CLEAR selection using methods included with DESeq2. Each comparison was processed with the SciKitLearn (40) PCA implementation and plotted using custom scripts in Python.

RESULTS

Quality of lcrRNA-seq libraries from serial dilutions of total RNA derived from FACS-derived cells strongly depends on input RNA mass

The experimental design for developing the CLEAR workflow is presented in Figure 1a. Our goal is to isolate the effect of limiting amounts of input material on the ability to detect differences between two biological conditions from small numbers of replicates. Total RNA was extracted from FACS-derived primary CD5+CD19+ (CD5+) and CD5-CD19+ (CD5-) cells from a single chronic lymphocytic leukemia (CLL) patient whose blood samples contained both cell types at disease diagnosis. The resultant total RNA was diluted to levels representing amounts found in typical lcrRNA-seq projects with three replicates for each input mass (10-, 100-, and 1000-pg) and each condition (CD5+ and CD5-). Although CLEAR is targeted for between-group comparisons in rare/limiting cell transcriptomes, sample inputs used for its development were from extracted total RNA and not from cell pools. The design rationale is as follows: 1) To track the efficacy of transcripts selected by CLEAR in downstream DESeq2 analysis, the composition of the input RNA source had to be the same for all dilutions. In this case, the only difference between input levels within the same cell types was the input RNA amount. This criterion cannot be achieved by using cell pools (i.e., transcriptomic profiles of pools of 10 cells or even 100 cells may be different due to real biological variations in the cells making up the pools); 2) The two lower levels of input RNA (10- and 100-pg) were chosen to represent RNA amounts from ~5 and ~50 cells, respectively. The 1,000-pg input level was chosen as a 'gold standard', where systems noise from this RNA input amount, though still considered as low, should be minimal (10). lcrRNA-seq data from 1,000-pg will allow us to ascertain if data from lower input levels are sufficient to provide adequate reliable signals to support differential gene expression analysis; 3) Primary immune cells are known to contain very low amounts of RNA. The CLL patient blood sample used in CLEAR development was processed and banked by the OSUCCC Leukemia Tissue Bank. Therefore, RNA degradation resulting from sample preparation (i.e., collection, processing, and storage steps as well as thawing, surface marker-labeling and FACS-enrichment steps) would be reflected in the transcript coverage profiles utilized in the CLEAR transcript selection process. This mimics the sample quality of a typical clinical study better than cell line-derived RNA.

Global preamplification of total RNA was performed using the SMARTer Ultra Low RNA V4 Kit (Takara/Clontech) followed by Illumina sequencing library generation using the Nextera XT kit (Illumina). We obtained an average of 15.5 million pass filter clusters with a range from 13.4 to 17.4 million, which is comparable to the read depths used in bulk mRNA-seq experiments. Data preprocessing steps and post-alignment data quality assessment were similar to those used in processing bulk RNA-seq data. In Figure S2, we present a selection of informative quality control (QC) parameters to illustrate the effect of input RNA amounts on the amount of usable information from lcrRNA-seq data. Specifically, the nine parameters (alignment rates, unique alignment rates, positional duplication rates, exonic rates, intronic rates, intergenic rates, number of transcripts represented in the aligned data, the strandedness rates, and percentage of trimmed sequence clusters represented by the top 30 expressed transcripts) are informative regarding data complexity and genome/transcriptome coverage. Not surprisingly, QC parameters clearly correlate with RNA input amounts signifying that ultralow RNA input mass at 10- and 100-pg levels severely reduce transcriptomic information from lcrRNA-seq data even though samples from all three input levels were sequenced to similar depths.

Low input RNA-seq data from two groups of serially diluted samples result in dissimilar differentially expressed genes when processed using a standard RNA-seq pipeline

In order to examine the effect of technical noise associated with ultralow input RNA amounts in lcrRNA-seq experiments, we performed gene expression analysis using a standard bulk cell RNA-seq workflow (generally for libraries derived from 100 - 200ng input mass) on the 10-, 100- and 1000-pg replicates without consideration of noise structure such as signal dropouts, RNA degradation, and high read duplication rates. As expected, the overall transcript variabilities, depicted in Figure S3 as scatterplots between replicates of the two cell types, were highest in the 10-pg input RNA replicates. In all of the samples, variabilities were highest in the low to medium expressed transcripts while the expression profiles converged at highly expressed transcripts.

Next, we performed differential gene expression analysis using a DESeq2 workflow without modifications. In Figure 1b, differentially expressed gene (DEG) counts for the CD5+ vs. CD5- comparison were: 1,000-pg: 2996, 100-pg: 744, and 10-pg: 898. This outcome is unexpected, as the statistical power to discern DEGs should increase with increasing RNA input mass. When we examined DEGs between the cell types shared by the three input amounts (Figure 1c), we observed a low number of shared DEGs between any two input levels. This is also unexpected because the three input levels were prepared from the same CD5+ and CD5- total RNA stocks. In Figure 1d, we present PCA plots for cell type comparisons at the three input levels. Clearly, at the 10-pg input amount, the gene expression profiles from the three CD5- replicates were vastly different from each other resulting in no separation between the cell types at either Principal Component 1 (PC1) or PC2. At the 100- and 1,000-pg levels, the gene expression profiles distinguished the two cell types with PC1 accounting for 26.3% and 74.6% of the variance, respectively.

Taken together, the gene expression profiles, the DEG dissimilarities and quantities, and the inconclusive PCA outcome reveal a high degree of systems noise at the 10-pg input level. At the 100- and 1,000-pg input amount, systems noise associated with lcrRNA-seq library generation was less dramatic but still contained variabilities as depicted by the low number of shared DEGs. As such, gene expression analysis for lcrRNA-seq requires a custom approach to control for systems noise.

Individual gene coverage profiles can guide selection of robust and reliably quantifiable transcripts in high noise conditions

It is known that systems noise/artifacts associated with global preamplification of ultralow input RNA-seq library generation are most apparent in lowly expressed transcripts and are manifested as high amounts of duplicated reads (14, 41) (see representative read pileups in transcripts not passing CLEAR assessment as depicted in Figure 2). As our aim is to provide a DEG analysis workflow for samples characterized by low RNA content (e.g., immune cells or quiescent cells) and degraded RNA (e.g., samples collected from multi-steps processes or challenging samples such as wound fibroblasts), we elect to identify reliable transcripts that are less affected by the library generation approach in each

replicate within each experimental group for downstream between-group comparisons. The resultant CLEAR workflow is presented in Figure 2a.

In Step 1, processed reads (adapter- and quality trimmed reads followed by removal of high abundance transcripts such as ribosomal RNAs and mitochondrial RNAs) are aligned to the reference genome (the entire human genome in this instance).

In Step 2, genomic alignment information is used to derive μ_i , the mean of positional read distribution along each transcript represented in the data. The expectation of intact transcripts with an even read distribution profile (i.e., little to no reads piling up towards either ends of the transcript (42)) will have a $\mu_i \approx 0$. With decreasing total RNA input mass, presence of degraded RNA becomes more apparent in the resultant data. This manifests as μ_i progressively deviating from 0 (even distribution) to -1 (reads building up on 5' ends of transcripts) and +1 (reads building up on 3' ends of transcripts).

In Step 3, we seek to identify transcripts affected by systems noise by ordering and binning genes by their respective expression rate. The bin size selected for this visual stratification is 250 transcripts and bins are ordered from the highest- to the lowest expression rates. The aggregate μ_i profiles for all available bins are presented as violin plots for ease of visualization. The aggregate fragment means distributions undergo a transition from $\mu_i \approx 0$ to $\mu_i \neq 0$. By presenting μ_i in this manner, we are able to visually gauge the quality of lcrRNA-seq data within replicates and between sample groups by noting the transcript rank index at which this transition takes place.

In Step 4, we capture this shift of aggregate μ_i from a unimodal distribution centering around the midpoint of the transcript to a bimodal distribution favoring both ends of the transcript by calculating the parameter t . This is accomplished by modeling the transition using individual fragment distribution profiles for all transcripts within each bin as described in Equation 2 in the Methods section.

In Step 5, we observe the transition in the model parameter t as transcript expression is varied from high to low. We identify transcripts with a threshold value of 0.5, whereby transcripts with higher expression than this value is used for downstream analysis such as hierarchical clustering, PCA and DEG analysis (Step 6). Transcripts with expression lower than this threshold are deemed too impacted by noise to be used for between-group comparisons.

In Figure 2b, we illustrate the approach by showing the read coverage profiles for three different genes. The first, GAPDH, is a highly-expressed housekeeping gene. We note the evenness of read coverage of highly expressed genes in lcrRNA-seq data, similar to that found in bulk RNA-seq. The gene coverage profile for the second gene, RPS7, is in the final expression bin accepted at the transition point of $t = 0.5$. At this point, gene coverage profiles switch from acceptable unimodality centering at the middle of the transcript to unacceptable amounts of bi-modality whereby transcript coverage starts to reveal location(s) with read pileups and location(s) with little to no read coverage, a phenomenon well depicted in the RPS7 coverage. Lastly, gene DDAH2 is below the threshold $t = 0.5$. As presented, the read coverage profile is dominated by regions of high coverage with vast sections of no coverage. This type of read coverage profile tends to provide erroneous gene expression quantifications, leading to the false calling of DEGs.

In Figures 2c (scatterplots) and 2d (violin plots), we show the behavior of the coverage means μ_i for one replicate of each of the CD5+ dilution input, which was used in the development of the CLEAR algorithm. Panel c shows the coverage means μ_i for each of the 7,000 highest expressed primary transcripts at each input RNA concentration. Panel d shows the same data with bins of 1,000 genes represented by violin plots. The 1,000- and 100-pg samples show an even read distribution for the 7,000 highest expressed transcripts while the 10-pg samples display a bifurcation from unimodality to bimodality. The red line indicates the transition point between robustly quantified- and noisy transcripts, as determined by the CLEAR algorithm. Due to the higher total RNA input amount, the data quality for the 100- and the 1,000-pg dilution samples is much better; thus, their transition points occur at transcripts

with lower expression rates than those of 10-pg input mass and are not visible in the figures showing only the 7,000 highest expressed transcripts.

CLEAR selection improves overlap of differentially expressed genes between CD5+ and CD5- samples at all three input dilution levels leading to cell type separation even at the 10pg level

CLEAR is designed to identify robust full-length transcripts from lcrRNA-seq data for DEG analysis. We utilize the CD5+/CD5- dilution experiment to illustrate this workflow. Earlier in this report (Figure 1b-d; Figures S2-S3), we presented the impact of systems noise associated with ultralow input patient RNA-seq libraries prepared with global preamplification approaches. In Figures 3 and S5, we presented evidence for the transformative power of removing noisy transcripts in lcrRNA-seq DEG analysis using CLEAR. The first step in understanding the impact of CLEAR on data quality in relationship to input amounts is to examine the number of CLEAR transcripts for each sample for downstream analyses. The red bars in Figure 3a show that there are 15,974 CLEAR transcripts shared between all six 1,000-pg samples (three CD5+ replicates and three CD5- replicates). This number drops to 7,655 for the 100-pg samples and to 407 for the 10-pg samples. This highlights that for the 100-pg and 1000-pg samples, most CLEAR transcripts are shared among all six samples, while, for the 10-pg samples, most CLEAR transcripts are unique to one of the six samples. This illustrates the susceptibility to systems noise when input amount is at 10 cells or below. The same trends are observed when the shared CLEAR transcripts are investigated separately by cell type (Figure S4).

The effect of the CLEAR algorithm on replicate-to-replicate comparisons is presented in Figure S5. The most striking first impression is that CLEAR removes a large number of lowly expressed transcripts from the 10-pg input level leaving mainly highly expressed transcripts for downstream analyses. The amount of retained transcripts increases with increasing RNA input mass. For the 1,000-pg samples, we observe transcripts from the entire transcription range passing CLEAR assessment. This supports ours and others' postulation (10) that the molecular complexity in 1 ng RNA starts to approach those found in bulk RNA-seq. We note that each pair of comparisons has a slightly different scattering profile, showing that CLEAR is assessing the means μ_i and the bimodality t in each sample independently so that the transcript removal criterion is set by data quality of each replicate in each input mass and cell type and not by a static cutoff value.

The Venn diagrams in Figure 3b show the overlaps between CLEAR transcripts common to all 6 samples (3 replicates each of CD5+ and CD5-) within each RNA input level (depicted by the red bars in Figure 3a). The CLEAR algorithm has distinctly done its job in excluding noisy transcripts from the lcrRNA-seq data at all three RNA input levels. This results in nearly all of the shared CLEAR transcripts at each input level to be contained in the shared CLEAR transcripts of the respective higher input levels.

The same consistency between input levels remains for DEGs as shown in the histogram in Figure 3c and the Venn diagram in Figure 3d. In contrast to the analysis without CLEAR in Figure 1b (repeated as *inset* in Figure 3c), the number of DEGs is now lowest ($n=3$) in the 10-pg comparison, intermediate ($n=189$) in the 100-pg comparison, and largest ($n=2,826$, i.e., over 10-fold more than in the 100-pg samples) in the 1,000-pg comparison. This trend is expected from the increasing quality of the lcrRNA-seq data. Also, the Venn diagram depicting the overlap between DEGs at different input RNA levels is different from that shown in Figure 1c. When only CLEAR transcripts are used (Figure 3d, *bottom* Venn diagram), of the 3 DEGs at the 10-pg input levels, CD69 is reproduced in all three comparisons, SRSF11 is reproduced in the 1,000-pg comparison, and HINT1 is not reproduced in the other comparisons. Of the 189 DEGs at the 100-pg input level a majority ($n=136$) is shared with the 1,000-pg input level, in contrast to the analysis without CLEAR in Figure 1c (repeated as *top* Venn diagram in Figure 3d), where more DEGs were unique to the 100-pg input level than shared with the 1,000-pg input level. We also performed PCA using CLEAR transcripts from the two cell types at all three input levels and the outcomes are shown in Figure 3e. Unlike its counterpart in Figure 1d (PCA of 10-pg from Figure 1d repeated as *inset* in Figure 3e), the CD5+ triplicates are now separated from the CD5- triplicates along PC1 even at the 10-pg input level. The separations observed at the 100- and 1,000-pg levels in Figure 3d are about the same as those in Figure 1d.

In the above comparisons, it is important to remember that the dilution samples were prepared from the same total RNA stock solution and the library generation was performed using the same reagent kits, by the same scientist, at the same time, and sequenced on the same flow cell. The dramatic differences in data quality observed in Figure 2c - 2d are mainly associated with the input RNA amount. While the straightforward analysis shown in Figure 1 is severely hampered by the amount of systems noise in the low input samples, by using CLEAR we are able to rescue differential gene expression analysis even for the lowest input amount.

The number of CLEAR transcripts correlates with authors' quality measures in publicly available scRNA-seq data sets

The next step in the CLEAR algorithm's development was to evaluate its effectiveness in assessing data quality in publicly available ultralow input RNA-seq data sets. Since CLEAR is designed to work with full length mRNA-seq data derived from extremely low amounts of RNA, we focused on data generated using the SMART approach. In a recent publication, Ilicic et al. (23) described a tool utilizing a machine learning algorithm to remove data derived from low quality/degraded cells so that they would not result in misleading conclusions. The scRNA-seq data Ilicic et al. (23) used for their tool development were generated by a Fluidigm/SMART-seq-based approach and well-annotated with the authors' assessment of each cell's quality classification. Out of the cell types evaluated in this study, we selected the mouse embryonic stem cells (869 cells with data, out of which we used 576 cells grown in either 2i or alternative 2i media for the CLEAR comparison; data derived from control media were not used) to compare CLEAR's assessments of their quality with the quality calls (captured cell quality calls of: a) good; b) empty or no capture; c) multiple cells; d) debris only) by the authors. In Figure 4a, we present violin plots illustrating the read coverage means μ_i from one of the scRNA-seq data from the 'Good' category. It is evident that the μ_i bifurcations observed in our CD5+/CD5- lcrRNA-seq data are also observed in Ilicic et al.'s scRNA-seq data (23). In Figure 4b, we provide the distributions of CLEAR transcript counts for each of the four captured cell quality calls. For the 521 'Good' cells, the range of CLEAR transcripts was tight with most cells having mean CLEAR transcript counts of 6,103. Not surprisingly, we are able to obtain the highest number of cells with usable data from this quality category.

Since scRNA-seq leverages information from hundreds of cells for cell type classifications, the transcriptome information from individual cells (generally with sequencing depths of a few millions reads or less) are not always adequate for transcript coverage assessment. Thus, even some cells in the 'Good' category do not have sufficient transcript complexity/coverage for a significant number of transcripts to pass CLEAR assessment. Similarly, many of the cells with 'Empty' designations (33% out of 15 tested) have zero CLEAR transcripts, explaining the wide transcript count distribution profile that bottomed out at zero. The mean CLEAR transcript count in this category is 1,565; however, that value is likely driven up by two outlier (possibly misclassified) cells with 6,010 and 6,940 CLEAR transcripts. In all, the transcripts observed in this category likely were derived from 'ambient' mRNA, i.e., RNAs from broken cells, which is latent in cell suspension solution. The transcript distribution profiles are therefore bottom heavy with a few cells having values close to the mean value of the 'Good' group. Although the 'Multiple' group has mean CLEAR transcript counts similar to that of the 'Good' group, the overall profile from the 16 cells is more top-heavy signifying that the presence of >1 cell (therefore more total RNA) led to deeper profiling of the transcriptome. The group described as 'Debris' (n=24) has a distribution profile intermediate between the 'Good' and the 'Multiple' groups. The mean CLEAR transcript values for these three groups are very similar to the 'Debris' group having a broader distribution profile than the 'Good' group. It is likely that some of the 'Debris' cells were broken subsequent to capture thereby the cell contents, including the RNAs, were actually present leading to successful scRNA-seq library generation. In all, it makes sense that the spread of the CLEAR transcript profiles for the 'Multiple' and the 'Debris' groups are much broader than the 'Good' and the 'Empty' groups as it is likely more difficult to visually discern the 'Multiple' and 'Debris' categories than to call the 'Good' and 'Empty' categories.

The number of CLEAR transcripts is similar between studies with similar input RNA mass

We selected a second data set from a recent study by Bhargava et al. (14), which reports the evaluation outcomes of several RNA preamplification approaches for low input RNA-seq: SMART-seq,

DP-seq and CEL-seq. For consistency, we selected the RNA-seq data derived from SMART-seq to evaluate CLEAR. Library generation input in this study was prepared from serial dilution (25-, 50-, 100- and 1,000-pg) of polyA-selected mRNA from control and Activin A-treated mouse embryonic stem cells. Once again, to depict that the μ_i bifurcations observed in the CD5+/CD5- lcrRNA-seq data also occurred in Bhargava et al. (14) lcrRNA-seq data, we show the read coverage mean μ_i from sample SRX350916 (25-pg SFM) in Figure 4c. It is evident that the shift from a unimodal to a bimodal distribution is also observed in this data set. Figure 4d presents the CLEAR transcript counts for the four samples (two replicates each of control and treated groups) at the four mRNA input levels. As expected, the number of CLEAR transcripts increases with increasing amount of input mRNA. It is also worth noting that there were differences in the spread of the shared CLEAR transcripts among the four samples at each mRNA level. We then asked if the number of CLEAR transcripts in the Bhargava et al. (14) data were similar to that of our CD5+/CD5- data at the different RNA input levels. An important detail to note is that the input values in the Bhargava et al. (14) data were polyA-selected mRNA whereas the CD5+/CD5- data were total RNA. Given that a large majority of RNA in a total RNA preparation is ribosomal RNA, 10 is a conservative conversion factor (43) between total RNA and mRNA input amount. Using this conversion factor, our 1,000-pg total RNA 'gold standard level' is equivalent to Bhargava et al.'s (14) 100-pg of mRNA input. Interestingly, the shared CLEAR transcripts among the 6 1000-pg CD5+/CD5- replicates were 15,974 and the Bhargava et al. (14) 100-pg mRNA input samples ($n = 4$) had a similar order (mean 14,823) of CLEAR transcripts as well. At the intermediate input level of 100-pg, the corresponding level for the Bhargava et al. study would be a mRNA input level of 10-pg. Since their lowest input level was 25-pg with average CLEAR transcript counts of 10,403, this puts the average CLEAR transcripts of 7,655 in our 100-pg data in a similar range as projected from the Bhargava et al. (14) 25-pg data. Due to the higher RNA input amount (the lowest input mass of 25pg mRNA would correspond to ~250pg total RNA) and that only RNA molecules with intact poly(A) tails were used for library generation, the data in the Bhargava et al. (14) study was not challenging enough to highlight CLEAR's ability to improve DEG and PCA analyses between the two biological groups in this study (data not shown).

CLEAR improves PCA separation of three types of murine neural cells and identifies genes known to be differentially expressed between cell types

To demonstrate the applicability of CLEAR in a biological system, lcrRNA-seq was used to transcriptionally profile different cell populations of the murine hippocampal dentate gyrus (DG), a highly studied neurogenic niche in the brain that is associated with memory and cognitive function (44). This region is of particular interest because resident stem and glial cells show robust morphologic and proteomic responses to a variety of injuries such as trauma and seizures (45, 46). Unfortunately, the stem cells and local glial populations are small cell populations embedded in a heterogeneous niche. Their isolation can be achieved using genetic and cell surface markers, but the cell yields are limiting. Previous transcriptomic studies have relied largely on scRNA-seq or pooling of up to 10 mice per sample to characterize these cell populations, but many experimental questions focus on population level changes in transcript expression and require multiple biological replicates (47–52). For these reasons, single cell data and traditional bulk sorting are impractical. Instead, for studies seeking population-level expression data, capturing the transcriptomes of a small sample of each cell type from several individual mice would be the ideal method for quantifying transcriptional changes.

As outlined in the Methods section, DGs were harvested from Nestin-GFP mice and sorted on the basis of fluorescent reporter expression and cell surface protein immunostaining to enrich for astrocytes, neural progenitors, and neural stem cells using FACS. As these cells are limited, transcriptome analysis would normally require the pooling of DGs from several mouse brains to yield sufficient RNA as input for bulk RNA-seq. By implementing the preamplification-based lcrRNA-seq approach and using CLEAR to select robust transcripts not affected by systems noise, one mouse brain per biological replicate provided ample cell yield for sequencing. The goal of this study was to evaluate the cell type enrichment by identifying genes which are known to be preferentially expressed in each cell type. The study schematics of enriching and generating lcrRNA-seq libraries from neural stem cells, progenitors, and astrocytes is shown in Figure 5a. The numbers and variabilities of CLEAR transcripts among replicates between the three cell types are displayed in Figure 5b. In the three cell types, it is evident that the progenitor cells yielded the highest numbers of CLEAR transcripts, with stem cells yielding intermediate amounts, and

astrocytes the lowest amounts. While this trend may reflect differences in cell size and RNA content, it may also reveal the tolerance of each cell type toward the cell dissociation and enrichment conditions. For example, astrocytes possess a complex branching of fine processes extending from their cell body that could be damaged during the mechanical dissociation and flow sorting steps. Furthermore, they are intrinsically reactive to changes in the external environment (53) which could include the chemical dissociation step and FACS processing in phosphate-buffered saline devoid of fetal bovine serum, Ca^{2+} , and Mg^{2+} to be compatible with direct preamplification with the Clontech SMARTer preamplification kit. The low number of CLEAR transcripts associated with this cell type may reflect a higher sensitivity to the cumulative stress caused by the sample preparation steps.

Application of CLEAR greatly enhanced separation of the three cell populations, despite suboptimal cDNA quality from the astrocyte population, compared to analysis using all available transcripts. To illustrate this, we compare PCA plots with all available transcripts vs. only CLEAR transcripts. When all transcripts were used, PCA plots show a clear distinction between stem and progenitor cells (Figure 5c third panel on *top*), but the lower transcript quality in astrocytes made the discrimination between astrocytes and stem cells unclear (Figure 5c first panel on *top*). In spite of the lower quality of the astrocyte transcripts, astrocytes and progenitors are still well separated due to the drastic differences in transcript profiles between the two cell types (Figure 5c second panel on *top*). Upon application of CLEAR, we are able to reveal the separation between astrocytes and stem cells (Figure 5c first panel on *bottom*) while retaining the separation between astrocytes and neural progenitors (Figure 5c second panel on *bottom*).

Genes that are known to be differentially expressed in murine neural stem cells, progenitors and astrocytes are used to confirm the identity of the cell populations derived from staining and FACS enrichment (Figures 5d, S6 and Table 1). Due to the CLEAR transcript assessment criterion, transcripts with low- to no sequencing reads would be precluded from the downstream analyses. These low- to no sequencing read coverage profiles can be a result of transcript dropouts, non-expressed or lowly expressed genes, or library preparation artefacts. As such, out of the list of known transcripts discussed here (Table 1), only the following genes have CLEAR transcripts in all three cell types for downstream analysis (Figure 5d): glial fibrillary acidic protein (*Gfap*), HOP homeobox (*Hopx*), fatty acid binding protein 7 (*Fabp7*), glutamate ionotropic receptor NMDA type subunit 2C (*Grin2c*), and SRY-Box 9 (*Sox9*). The outcome of the DESeq2 comparisons are summarized in Table 1. Genes that do not have CLEAR transcripts (Failed CLEAR or FC) are also included for review (Figure S6 and Table 1).

Out of the three cell types, it is known that progenitors are more distinct in gene expression profile while astrocytes and stem cells are less distinguishable (48, 49). At the known transcript level, *Gfap* and *Sox9* (2 of the 4 genes that pass the CLEAR criterion) are known to be higher in astrocytes and stem cells than progenitors. As expected, we found that GFAP and *Sox9* were significantly higher in FACS-isolated stem cells than progenitors ($q < 0.01$ and 0.0001 , respectively). The expression levels for these two genes were not significantly different between astrocytes and progenitors, but their transcription levels in astrocytes are closer to stem cells than to progenitors. Two additional genes, inhibitor of DNA binding 4 (*Id4*) and SRY-Box 2 (*Sox2*), are known to have similar transcript levels in astrocytes and stem cells, both of which are higher than in progenitors. Although the read coverage profiles for these two genes failed the CLEAR criterion, the overall normalized counts are more similar between astrocytes and stem cells than with progenitors. Overall, these four known transcripts verify that the sorted stem- and astrocyte populations are distinct from the progenitor population.

Two genes, glutamate ionotropic receptor NMDA type subunit 2C (*Grin2c*) and HOP homeobox (*Hopx*), are known to be differentially expressed between stem cells and astrocytes. Both of these genes pass the CLEAR criterion. *Hopx* is expected to be higher in stem cells and this was indeed the case (Figure 5d and Table 1; $q < 0.01$). *Grin2c* is expected to be higher in astrocytes and this was also substantiated by DESeq2 analysis (Figure 5d and Table 1; $q < 0.001$). Also as expected, our data show that the expressions of *Hopx* and *Grin2c* are significantly higher in stem cells and astrocytes, respectively, than progenitors (Figure 5d and Table 1; $q < 0.0001$). In addition, the expression of *Fabp7* is known to be higher in stem cells and progenitors relative to astrocytes. The expression levels of *Fabp7* are significantly higher in progenitors and stem cells when compared to astrocytes ($q < 0.01$ and $q < 0.05$,

respectively) and the levels between progenitors and stem cells are not significantly different. Despite stem cells and astrocytes having markedly different biological functions, isolating these two cell populations *ex vivo* is a challenging task due to highly overlapping gene expression profiles (48). These data confirm that lcrRNA-seq with CLEAR can effectively distinguish these difficult to separate populations.

Lastly, the remaining group of genes depicted in Figure S6 and Table 1, are also known to be important in the discrimination between these three cell types. A low number of these genes pass CLEAR analysis, and they are marked with asterisks. They include genes that are enriched in the progenitor population such as *Mcm2*, *doublecortin (Dcx)*, *eomesodermin (Eomes)*, *proliferating cell nuclear antigen (Pcna)*, *neuronal differentiation 1 (Neurod1)*, and *neurogenin 2 (Neurog2)*. Close examination of normalized counts plots shown in Figure S6 reveals a distinct trend that these 5 genes have higher expressions in the progenitors, as expected (47–51, 54). *Nestin (Nes)* is expected to be expressed in both stem and progenitor cells but is only observed in progenitor cells; this highlights the importance of a custom approach to lcrRNAseq, as this comparison would be interpreted as a significant difference ($q \leq 0.01$ in the comparison without CLEAR preprocessing), whereas CLEAR identifies it as failing in all three cell types. Taken together, our dataset recapitulates and reinforces relative gene expression patterns reported in the field for neural stem cells, progenitors, and astrocytes and shows that lcrRNA-seq with CLEAR can be used to distinguish murine neural astrocytes, progenitors, and stem cells.

DISCUSSION

Total RNA input amount for limiting-cell RNA-seq (e.g., 10 - 1,000-pg from 5 - 100 cells) is closer to the amount found in single-cell RNA-seq studies (2 - 100-pg) than to bulk RNA-seq studies (100 - 200-ng). Due to the minute amount of RNA found in single-cell and limiting-cell transcriptomic studies, the library generation process, with the exception of single-molecule sequencing, is preceded by global cDNA preamplification. Researchers have observed artefacts such as a large proportion of the sequencing reads being dominated by a small number of transcripts (14), excessive transcripts with zero read counts (55), high variabilities between samples and within replicates of the same sample (56), distortion towards shorter transcripts due to poor amplifications of longer transcripts (57), and higher observed variances at lower biological abundances (10, 11). Together, these artefacts result in noisy scRNA-seq and lcrRNA-seq data that challenge a number of the assumptions that are fundamental to bulk RNA-seq analysis approaches and render them unsuitable for direct application to single-cell and limiting-cell data (16). In order to overcome some of these challenges associated with systems noise, strategies currently being used to uncover important biological differences in single cell or rare cell populations include: 1) identifying low-quality, high-noise samples and removing them from downstream analyses (23); 2) applying transcript normalization (16, 26, 28, 58); 3) incorporating ERCC spike-in control (56, 59); 4) utilizing median absolute deviation (which is more resistant to outliers) to characterize statistical dispersion (12); 5) integrating UMIs to track transcripts by molecular counts (60). Yet, due to the often-low number of replicates and the goal of identifying differences in gene expression profiles between two groups, the strategies for scRNA-seq data just described are not entirely appropriate or adequate for lcrRNA-seq data.

In this paper, we describe CLEAR, a simple and objective approach to identify transcripts in lcrRNA-seq with acceptable systems noise for downstream data analysis. CLEAR requires transcripts to be reliably quantifiable in all replicates within and across treatment/control- or cell-type groups. This requirement is possible for lcrRNA-seq data due to the RNA quality preservation effects of recent improvements in direct preamplification reagents and their delivery using nanoliter microfluidics devices. These technical advances eliminate the need to extract RNA leading to lower RNA degradation and higher RNA yield as well as faster reagent deliveries and more thorough reagent/RNA mixing in microwell plates when used with microfluidics devices. The resultant improvement in RNA quality contributes to even read coverage in lcrRNA-seq data.

To the best of our knowledge, utilizing CLEAR to preprocess lcrRNA-seq data followed by DEG analysis is unique and unlike computation approaches used by others in their ultralow RNA-seq studies. For example, Shanker et al. (13) performed Pearson correlation comparisons between serial dilutions of input RNA vs. their 1 μg input control using \log_2 of median RPKM for all genes having ≥ 2 reads coverage. Bhargava et al. (14) performed DESeq without prior data preprocessing to compare the performance between three library preparation methods as well as within serial dilutions of mRNA derived from two mouse embryonic stem cell culture conditions. Liu et al. (61) utilized relative expression orderings or REOs to harmonizing clinical transcription signatures between low-input and bulk RNA-seq libraries. In contrast, CLEAR comprehensively screens all transcripts in all replicates within an lcrRNA-seq study for genes with even coverage profile for DEG analysis and other downstream analyses. The combination of characterizing each transcript by its own mean μ_i , derived from its positional read/fragment distribution, followed by choosing a cutoff defined by expression across the full distribution of transcripts is deliberate. For any given transcript, even one with low systems noise, there are many reasons why its mean μ_i could deviate from $\mu_i = 0$: 1) transposase-based library generation methods (62) do not efficiently 'tagment' the 5'-end of transcripts (the 3'-end is somewhat spared, likely due to the presence of the poly(A) tail) thereby resulting in coverage drop off at the 5'-ends; 2) the presence of various isoforms may skew the distribution of reads along the length of the transcript, especially when prominent isoforms are not correctly annotated (17); 3) truncated, polyadenylated RNA fragments/intermediates that are part way through the RNA decay pathway are captured (63); 4) RNA fragments with alternative polyadenylation sites are captured (17, 64, 65). Thus, the mean μ_i being different from zero by itself is not necessarily an indication that a transcript is affected by systems noise. Conversely, for some transcripts affected by systems noise their mean μ_i sometimes becomes more or less random and thus *can* be close to zero by chance. Simply keeping transcripts with a mean μ_i close to zero would result in some valid transcripts being excluded and some noisy transcripts being included. By characterizing the entire distribution of means μ_i over a defined range of expression levels, outliers due to the above-mentioned effects become obvious and do not affect the classification of the entire expression level. Instead of relying on a simple fixed cutoff at a particular expression level, the CLEAR approach adapts to the quality of individual samples to assess systems noise to select for robust transcripts for downstream analysis.

In the current work, we have selected two sets of publicly available data (14, 23) and one set of in-house data to illustrate the utility of CLEAR. One of the goals for the publicly available datasets was to show that the mean read/fragment distribution phenomenon observed in the CLEAR development data is also present in sc- and lcrRNA-seq libraries derived from Fluidigm C1 IFCs and manual SMART-seq, respectively. This is indeed the case as depicted by the violin plots in Figures 3d, 4a, and 4c where the distribution of the μ_i transitions from an acceptable distribution centered around 0 to an unacceptable broad/bimodal distribution. The other goal was to evaluate the ability of CLEAR to reveal and remove transcripts affected by the underlying systems noise from downstream analysis in a broad range of data sets. The application of CLEAR to the Illicic et al. scRNA-seq data (23) revealed interesting insights as discussed in the Results section. For example, Figure 4b displays the violin plots of the dispersion of CLEAR transcripts which captured characteristics associated with cell qualities evaluated by microscopy. When applied to the Bhargava et al. data (14), CLEAR identified increasing amounts of CLEAR transcripts with increasing mRNA input mass (Figure 4c) consistent with the observations in our own CD5+/CD5- data. Combined, these data confirm that CLEAR can independently reveal sample/transcript quality and identify highly degraded or noisy samples such as those derived from debris, empty wells or extremely low RNA input in Illicic et al. data (23) and increases in data quality with increasing level of RNA input mass in Bhargava et al. data (14).

To provide an example of implementing CLEAR in an in-house lcrRNA-seq study, we incorporated a proof-of-principle experiment with cells isolated from the neurogenic niche in the adult mouse hippocampus. Studying the hippocampal stem cell compartment in adult mice has been hampered by the limited number of stem and progenitor cells that can be isolated from a single mouse DG. Because of the low numbers of cells, transcriptome analysis has historically relied on single cells or the pooling of DGs from several mouse brains to collect sufficient cells for total RNA extraction and bulk RNA-seq (4–10). By implementing a preamplification-based lcrRNA-seq approach and using CLEAR to select robust

transcripts not affected by systems noise, we required only one mouse brain per biological replicate to achieve transcriptome profiling of clearly separated stem cells, progenitors and astrocytes. CLEAR greatly enhanced separation of the 3 cell types by PCA and targeted quantification of well-validated cell phenotype markers confirmed the identity of these 3 populations. This method will be particularly useful for studies of population level transcriptome changes in experimental injury models, where inter-subject variability necessitates sequencing multiple subjects and pooling of mice is unfavorable for practical and ethical reasons.

When comparing different biological groups, it is possible that a gene is highly expressed in one group but not the other. An example of this can be seen in the *Eomes* gene in Figure S6, which passes CLEAR in the progenitors and fails in the other two cell types. While true DEG analysis is not possible for such genes, one can still use the CLEAR cutoff expression level (the count of the lowest transcript passing CLEAR for a particular sample) to report a bound on the fold change of such a gene consistent with the CLEAR analysis. As an example, comparing Astrocyte and Progenitor expression of *Eomes*, DESeq2 reports a \log_2 fold change of 8.97, whereas the bounding procedure above suggest a more modest difference of 6.84. This analysis should be more reliable than extreme fold changes due to zero or near zero counts (dropouts) reported by DESeq2 if applied to all transcripts.

Although CLEAR can be applied to scRNA-seq data just as effectively as lcrRNA-seq data (Figure 4, results from analyzing Illicic et al. (23) scRNA-seq data using CLEAR), the low complexity and high variability nature of scRNA-seq data would typically result in insufficient CLEAR transcripts for meaningful DEG analysis, especially when requiring transcripts to pass the CLEAR filter in all (usually of a very large number) of samples. Future research will focus on using imputation to relax the condition of passing the CLEAR filter in all samples for studies having large number of biological replicates.

In summary, utilizing a direct cDNA amplification approach, the lcrRNA-seq strategy allows researchers to perform global transcriptome profiling using limited numbers of cells. However, performing gene expression analysis on lcrRNA-seq data using computation approaches developed for bulk RNA-seq can lead to excessive amounts of false findings. To overcome this, the CLEAR algorithm is designed around two prevalent phenomena in ultralow input RNA-seq data: 1) a difference in systems noise due to global preamplification and RNA degradation between highly expressed and medium- to lowly expressed transcripts; 2) the read coverage profile of noisy transcripts contains discernible coverage gaps instead of even coverage along the transcript length. By gauging the average read coverage profile mean μ_i in transcripts binned by gene expression levels, CLEAR is able to systematically identify transcripts with sufficient integrity in all replicates and samples for downstream analysis.

As we explored publicly available datasets during the development of CLEAR, we also realized that by computing the means μ_i and displaying them as violin plots, CLEAR can be used as a visual QC tool to eliminate or set aside data from scRNA-seq samples that did not perform well at the cell enrichment stage or during the library generation process. In a related manner, by examining the overlapped CLEAR transcripts from 30- or 50-cell lcrRNA-seq with those from a 1ng input, researchers can assess whether they would need more cells or can get by with fewer cells to achieve an acceptable transcriptome profile seen in the 1ng 'gold standard'. In all, we highlighted the functionalities that CLEAR brings to sc- and lcrRNA-seq data preprocessing and data quality visualization and hope that this would spark additional computational and statistical development in this area.

AVAILABILITY

The Python code implementing CLEAR is available for download at <https://github.com/rbundschuh/CLEAR> under the GPL3 license.

All original sequencing files have been deposited to Gene Expression Omnibus (GEO) under accession numbers [PENDING PUBLICATION] (human CD5+ and CD5- data) and [PENDING PUBLICATION] (mouse neural data).

FUNDING

This work was supported in part by The Ohio State University Comprehensive Cancer Center and the National Institutes of Health (NIH) [P30 CA016058 (Genomics Shared Resource)]; the Pelotonia Foundation [fellowships to L.A.W., C.C, E.H.]; the NIH [R50 CA211524-03 to P.Y., CSBC/U54 grant to University of Texas Hlth. Sci. Ctr. - San Antonio via a subcontract GRT44526 to P.Y.]; an OSU Division of Hematology Seed Grant to P.Y. and N.M.; the Chronic Brain Injury and Discovery Themes at The Ohio State University [seed funding to E.K.]; and allocations of computation resources from the Ohio Supercomputer Center (66). Funding for open access charge: OSU Division of Hematology.

CONFLICT OF INTEREST

The authors declare that they do not have any competing interests.

REFERENCES

1. Tang,F., Barbacioru,C., Wang,Y., Nordman,E., Lee,C., Xu,N., Wang,X., Bodeau,J., Tuch,B.B., Siddiqui,A., *et al.* (2009) mRNA-Seq whole-transcriptome analysis of a single cell. *Nat. Methods*, **6**, 377–382.
2. Picelli,S. (2017) Single-cell RNA-sequencing: The future of genome biology is now. *RNA Biol.*, **14**, 637–650.
3. Kolodziejczyk,A.A., Kim,J.K., Svensson,V., Marioni,J.C. and Teichmann,S.A. (2015) The technology and biology of single-cell RNA sequencing. *Mol. Cell*, **58**, 610–620.
4. Ziegenhain,C., Vieth,B., Parekh,S., Reinius,B., Guillaumet-Adkins,A., Smets,M., Leonhardt,H., Heyn,H., Hellmann,I. and Enard,W. (2017) Comparative Analysis of Single-Cell RNA Sequencing Methods. *Mol. Cell*, **65**, 631–643.e4.
5. Haque,A., Engel,J., Teichmann,S.A. and Lönnberg,T. (2017) A practical guide to single-cell RNA-sequencing for biomedical research and clinical applications. *Genome Med.*, **9**, 75.
6. Ramsköld,D., Luo,S., Wang,Y.-C., Li,R., Deng,Q., Faridani,O.R., Daniels,G.A., Khrebtukova,I., Loring,J.F., Laurent,L.C., *et al.* (2012) Full-length mRNA-Seq from single-cell levels of RNA and individual circulating tumor cells. *Nat. Biotechnol.*, **30**, 777–782.
7. Picelli,S., Björklund,Å.K., Faridani,O.R., Sagasser,S., Winberg,G. and Sandberg,R. (2013) Smart-seq2 for sensitive full-length transcriptome profiling in single cells. *Nat. Methods*, **10**, 1096–1098.
8. Picelli,S., Faridani,O.R., Björklund,Å.K., Winberg,G., Sagasser,S. and Sandberg,R. (2014) Full-length RNA-seq from single cells using Smart-seq2. *Nat. Protoc.*, **9**, 171.
9. Sasagawa,Y., Nikaido,I., Hayashi,T., Danno,H., Uno,K.D., Imai,T. and Ueda,H.R. (2013) Quartz-Seq: a highly reproducible and sensitive single-cell RNA sequencing method, reveals non-genetic gene-expression heterogeneity. *Genome Biol.*, **14**, R31.
10. Marinov,G.K., Williams,B.A., McCue,K., Schroth,G.P., Gertz,J., Myers,R.M. and Wold,B.J. (2014) From single-cell to cell-pool transcriptomes: stochasticity in gene expression and RNA splicing. *Genome Res.*, **24**, 496–510.
11. Streets,A.M., Zhang,X., Cao,C., Pang,Y., Wu,X., Xiong,L., Yang,L., Fu,Y., Zhao,L., Tang,F., *et al.* (2014) Microfluidic single-cell whole-transcriptome sequencing. *Proc. Natl. Acad. Sci. U. S. A.*, **111**, 7048–7053.
12. Wu,A.R., Neff,N.F., Kalisky,T., Dalerba,P., Treutlein,B., Rothenberg,M.E., Mburu,F.M., Mantalas,G.L., Sim,S., Clarke,M.F., *et al.* (2014) Quantitative assessment of single-cell RNA-sequencing methods. *Nat. Methods*, **11**, 41–46.
13. Shanker,S., Paulson,A., Edenberg,H.J., Peak,A., Perera,A., Alekseyev,Y.O., Beckloff,N., Bivens,N.J.,

- Donnelly,R., Gillaspay,A.F., *et al.* (2015) Evaluation of commercially available RNA amplification kits for RNA sequencing using very low input amounts of total RNA. *J. Biomol. Tech.*, **26**, 4–18.
14. Bhargava,V., Head,S.R., Ordoukhanian,P., Mercola,M. and Subramaniam,S. (2014) Technical variations in low-input RNA-seq methodologies. *Sci. Rep.*, **4**, 3678.
 15. Adiconis,X., Borges-Rivera,D., Satija,R., DeLuca,D.S., Busby,M.A., Berlin,A.M., Sivachenko,A., Thompson,D.A., Wysocker,A., Fennell,T., *et al.* (2013) Comparative analysis of RNA sequencing methods for degraded or low-input samples. *Nat. Methods*, **10**, 623–629.
 16. Vallejos,C.A., Risso,D., Scialdone,A., Dudoit,S. and Marioni,J.C. (2017) Normalizing single-cell RNA sequencing data: challenges and opportunities. *Nat. Methods*, **14**, 565–571.
 17. Grün,D. and van Oudenaarden,A. (2015) Design and Analysis of Single-Cell Sequencing Experiments. *Cell*, **163**, 799–810.
 18. Love,M.I., Huber,W. and Anders,S. (2014) Moderated estimation of fold change and dispersion for RNA-seq data with DESeq2. *Genome Biol.*, **15**, 550.
 19. van Dijk,D., Nainys,J., Sharma,R., Kathail,P., Carr,A.J., Moon,K.R., Mazutis,L., Wolf,G., Krishnaswamy,S. and Pe'er,D. (2017) MAGIC: A diffusion-based imputation method reveals gene-gene interactions in single-cell RNA-sequencing data. *bioRxiv*, 10.1101/111591.
 20. Trapnell,C., Cacchiarelli,D., Grimsby,J., Pokharel,P., Li,S., Morse,M., Lennon,N.J., Livak,K.J., Mikkelsen,T.S. and Rinn,J.L. (2014) The dynamics and regulators of cell fate decisions are revealed by pseudotemporal ordering of single cells. *Nat. Biotechnol.*, **32**, 381–386.
 21. McCarthy,D.J., Campbell,K.R., Lun,A.T.L. and Wills,Q.F. (2017) Scater: pre-processing, quality control, normalization and visualization of single-cell RNA-seq data in R. *Bioinformatics*, **33**, 1179–1186.
 22. Angerer,P., Haghverdi,L., Büttner,M., Theis,F.J., Marr,C. and Buettner,F. (2016) destiny: diffusion maps for large-scale single-cell data in R. *Bioinformatics*, **32**, 1241–1243.
 23. Ilicic,T., Kim,J.K., Kolodziejczyk,A.A., Bagger,F.O., McCarthy,D.J., Marioni,J.C. and Teichmann,S.A. (2016) Classification of low quality cells from single-cell RNA-seq data. *Genome Biol.*, **17**, 29.
 24. DeTomaso,D. and Yosef,N. (2016) FastProject: a tool for low-dimensional analysis of single-cell RNA-Seq data. *BMC Bioinformatics*, **17**, 315.
 25. Lin,P., Troup,M. and Ho,J.W.K. (2017) CIDR: Ultrafast and accurate clustering through imputation for single-cell RNA-seq data. *Genome Biol.*, **18**, 59.
 26. Finak,G., McDavid,A., Yajima,M., Deng,J., Gersuk,V., Shalek,A.K., Slichter,C.K., Miller,H.W., McElrath,M.J., Prlic,M., *et al.* (2015) MAST: a flexible statistical framework for assessing transcriptional changes and characterizing heterogeneity in single-cell RNA sequencing data. *Genome Biol.*, **16**, 278.
 27. Guo,M., Wang,H., Steven Potter,S., Whitsett,J.A. and Xu,Y. (2015) SINCERA: A Pipeline for Single-Cell RNA-Seq Profiling Analysis. *PLoS Comput. Biol.*, **11**, e1004575.
 28. Vallejos,C.A., Marioni,J.C. and Richardson,S. (2015) BASiCS: Bayesian Analysis of Single-Cell Sequencing Data. *PLoS Comput. Biol.*, **11**, e1004333.
 29. Kolodziejczyk,A.A., Kim,J.K., Tsang,J.C.H., Ilicic,T., Henriksson,J., Natarajan,K.N., Tuck,A.C., Gao,X., Bühler,M., Liu,P., *et al.* (2015) Single Cell RNA-Sequencing of Pluripotent States Unlocks Modular Transcriptional Variation. *Cell Stem Cell*, **17**, 471–485.

30. Schubert, M., Lindgreen, S. and Orlando, L. (2016) AdapterRemoval v2: rapid adapter trimming, identification, and read merging. *BMC Res. Notes*, **9**, 88.
31. Kim, D., Langmead, B. and Salzberg, S.L. (2015) HISAT: a fast spliced aligner with low memory requirements. *Nat. Methods*, **12**, 357–360.
32. O’Leary, N.A., Wright, M.W., Brister, J.R., Ciuffo, S., Haddad, D., McVeigh, R., Rajput, B., Robbertse, B., Smith-White, B., Ako-Adjei, D., *et al.* (2016) Reference sequence (RefSeq) database at NCBI: current status, taxonomic expansion, and functional annotation. *Nucleic Acids Res.*, **44**, D733–45.
33. Harrow, J., Frankish, A., Gonzalez, J.M., Tapanari, E., Diekhans, M., Kokocinski, F., Aken, B.L., Barrell, D., Zadissa, A., Searle, S., *et al.* (2012) GENCODE: the reference human genome annotation for The ENCODE Project. *Genome Res.*, **22**, 1760–1774.
34. Harrow, J., Denoeud, F., Frankish, A., Reymond, A., Chen, C.-K., Chrast, J., Lagarde, J., Gilbert, J.G.R., Storey, R., Swarbreck, D., *et al.* (2006) GENCODE: producing a reference annotation for ENCODE. *Genome Biol.*, **7 Suppl 1**, S4.1–9.
35. Liao, Y., Smyth, G.K. and Shi, W. (2013) The Subread aligner: fast, accurate and scalable read mapping by seed-and-vote. *Nucleic Acids Res.*, **41**, e108.
36. Kroll, K.W., Mokaram, N.E., Pelletier, A.R., Frankhouser, D.E., Westphal, M.S., Stump, P.A., Stump, C.L., Bundschuh, R., Blachly, J.S. and Yan, P. (2014) Quality Control for RNA-Seq (QuaCRS): An Integrated Quality Control Pipeline. *Cancer Inform.*, **13**, 7–14.
37. DeLuca, D.S., Levin, J.Z., Sivachenko, A., Fennell, T., Nazaire, M.-D., Williams, C., Reich, M., Winckler, W. and Getz, G. (2012) RNA-SeQC: RNA-seq metrics for quality control and process optimization. *Bioinformatics*, **28**, 1530–1532.
38. Wang, L., Wang, S. and Li, W. (2012) RSeQC: quality control of RNA-seq experiments. *Bioinformatics*, **28**, 2184–2185.
39. Quinlan, A.R. and Hall, I.M. (2010) BEDTools: a flexible suite of utilities for comparing genomic features. *Bioinformatics*, **26**, 841–842.
40. Pedregosa, F., Varoquaux, G., Gramfort, A., Michel, V., Thirion, B., Grisel, O., Blondel, M., Prettenhofer, P., Weiss, R., Dubourg, V., *et al.* (2011) Scikit-learn: Machine Learning in Python. *J. Mach. Learn. Res.*, **12**, 2825–2830.
41. Islam, S., Zeisel, A., Joost, S., La Manno, G., Zajac, P., Kasper, M., Lönnerberg, P. and Linnarsson, S. (2014) Quantitative single-cell RNA-seq with unique molecular identifiers. *Nat. Methods*, **11**, 163–166.
42. Feng, H., Zhang, X. and Zhang, C. (2015) mRIN for direct assessment of genome-wide and gene-specific mRNA integrity from large-scale RNA-sequencing data. *Nat. Commun.*, **6**, 7816.
43. Warner, J.R. (1999) The economics of ribosome biosynthesis in yeast. *Trends Biochem. Sci.*, **24**, 437–440.
44. Deng, W., Aimone, J.B. and Gage, F.H. (2010) New neurons and new memories: how does adult hippocampal neurogenesis affect learning and memory? *Nat. Rev. Neurosci.*, **11**, 339.
45. Weston, N.M. and Sun, D. (2018) The Potential of Stem Cells in Treatment of Traumatic Brain Injury. *Curr. Neurol. Neurosci. Rep.*, **18**, 1.
46. Kuruba, R., Hattiangady, B. and Shetty, A.K. (2009) Hippocampal neurogenesis and neural stem cells in temporal lobe epilepsy. *Epilepsy Behav.*, **14**, 65–73.

47. Artegiani,B., Lyubimova,A., Muraro,M., van Es,J.H., van Oudenaarden,A. and Clevers,H. (2017) A Single-Cell RNA Sequencing Study Reveals Cellular and Molecular Dynamics of the Hippocampal Neurogenic Niche. *Cell Rep.*, **21**, 3271–3284.
48. Hochgerner,H., Zeisel,A., Lönnerberg,P. and Linnarsson,S. (2018) Conserved properties of dentate gyrus neurogenesis across postnatal development revealed by single-cell RNA sequencing. *Nat. Neurosci.*, **21**, 290–299.
49. Dulken,B.W., Leeman,D.S., Boutet,S.C., Hebestreit,K. and Brunet,A. (2017) Single-Cell Transcriptomic Analysis Defines Heterogeneity and Transcriptional Dynamics in the Adult Neural Stem Cell Lineage. *Cell Rep.*, **18**, 777–790.
50. Shin,J., Berg,D.A., Zhu,Y., Shin,J.Y., Song,J., Bonaguidi,M.A., Enikolopov,G., Nauen,D.W., Christian,K.M., Ming,G.-L., *et al.* (2015) Single-Cell RNA-Seq with Waterfall Reveals Molecular Cascades underlying Adult Neurogenesis. *Cell Stem Cell*, **17**, 360–372.
51. Shi,Z., Geng,Y., Liu,J., Zhang,H., Zhou,L., Lin,Q., Yu,J., Zhang,K., Liu,J., Gao,X., *et al.* (2018) Single-cell transcriptomics reveals gene signatures and alterations associated with aging in distinct neural stem/progenitor cell subpopulations. *Protein Cell*, **9**, 351–364.
52. Sakai,A., Matsuda,T., Doi,H., Nagaishi,Y., Kato,K. and Nakashima,K. (2018) Ectopic neurogenesis induced by prenatal antiepileptic drug exposure augments seizure susceptibility in adult mice. *Proc. Natl. Acad. Sci. U. S. A.*, **115**, 4270–4275.
53. Liddelow,S.A. and Barres,B.A. (2017) Reactive Astrocytes: Production, Function, and Therapeutic Potential. *Immunity*, **46**, 957–967.
54. Zhang,J. and Jiao,J. (2015) Molecular Biomarkers for Embryonic and Adult Neural Stem Cell and Neurogenesis. *Biomed Res. Int.*, **2015**.
55. Lun,A.T.L., Bach,K. and Marioni,J.C. (2016) Pooling across cells to normalize single-cell RNA sequencing data with many zero counts. *Genome Biol.*, **17**, 75.
56. Brennecke,P., Anders,S., Kim,J.K., Kołodziejczyk,A.A., Zhang,X., Proserpio,V., Baying,B., Benes,V., Teichmann,S.A., Marioni,J.C., *et al.* (2013) Accounting for technical noise in single-cell RNA-seq experiments. *Nat. Methods*, **10**, 1093–1095.
57. Hayashi,T., Ozaki,H., Sasagawa,Y., Umeda,M., Danno,H. and Nikaido,I. (2018) Single-cell full-length total RNA sequencing uncovers dynamics of recursive splicing and enhancer RNAs. *Nat. Commun.*, **9**, 619.
58. Kharchenko,P.V., Silberstein,L. and Scadden,D.T. (2014) Bayesian approach to single-cell differential expression analysis. *Nat. Methods*, **11**, 740–742.
59. Ding,N., Melloni,L., Zhang,H., Tian,X. and Poeppel,D. (2015) Cortical tracking of hierarchical linguistic structures in connected speech. *Nat. Neurosci.*, **19**, 158.
60. Tung,P.-Y., Blischak,J.D., Hsiao,C.J., Knowles,D.A., Burnett,J.E., Pritchard,J.K. and Gilad,Y. (2017) Batch effects and the effective design of single-cell gene expression studies. *Sci. Rep.*, **7**, 39921.
61. Liu,H., Li,Y., He,J., Guan,Q., Chen,R., Yan,H., Zheng,W., Song,K., Cai,H., Guo,Y., *et al.* (2017) Robust transcriptional signatures for low-input RNA samples based on relative expression orderings. *BMC Genomics*, **18**, 913.
62. Gertz,J., Varley,K.E., Davis,N.S., Baas,B.J., Goryshin,I.Y., Vaidyanathan,R., Kuersten,S. and Myers,R.M. (2012) Transposase mediated construction of RNA-seq libraries. *Genome Res.*, **22**, 134–141.

63. Slomovic, S., Fremder, E., Staals, R.H.G., Pruijn, G.J.M. and Schuster, G. (2010) Addition of poly(A) and poly(A)-rich tails during RNA degradation in the cytoplasm of human cells. *Proc. Natl. Acad. Sci. U. S. A.*, **107**, 7407–7412.
64. Ha, K.C.H., Blencowe, B.J. and Morris, Q. (2018) QAPA: a new method for the systematic analysis of alternative polyadenylation from RNA-seq data. *Genome Biol.*, **19**, 45.
65. Elkon, R., Ugalde, A.P. and Agami, R. (2013) Alternative cleavage and polyadenylation: extent, regulation and function. *Nat. Rev. Genet.*, **14**, 496–506.
66. Ohio Supercomputer Center (1987) *Columbus OH: Ohio Supercomputer Center.* <http://osc.edu/ark:/19495/f5s1ph73>.

TABLES AND FIGURES

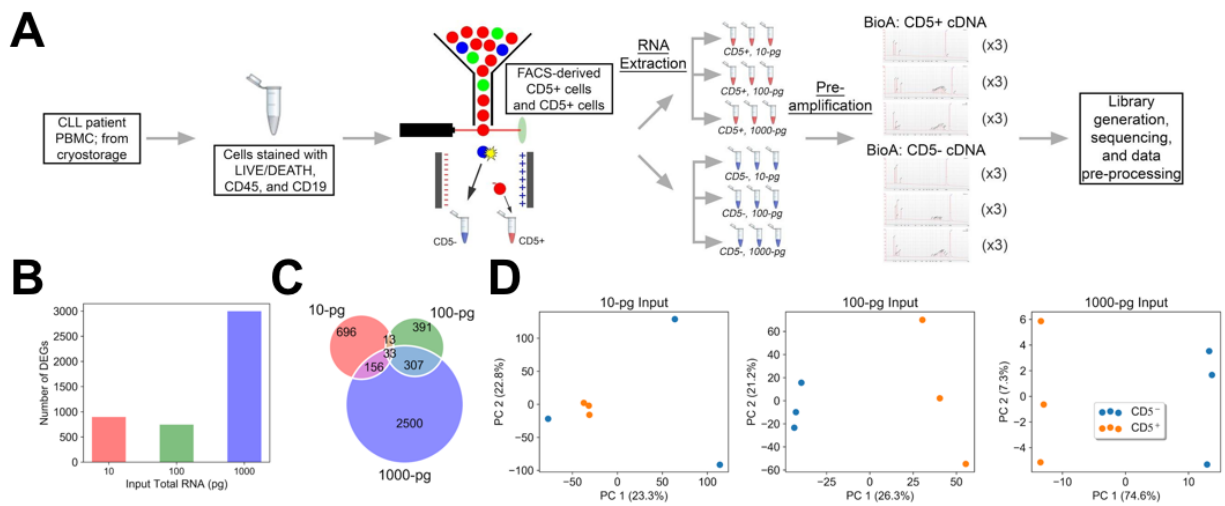


Figure 1

Figure 1. lcrRNA-seq analyses between sample groups without application of CLEAR. A) Workflow for total RNA extraction and QC analysis from FACS-derived CD5+ and CD5- CLL cells as input for lcrRNA-seq library generation for the development of CLEAR; **B)** The DEG counts as determined by DESeq2. Contrary to expectation, the 10-pg input has more DEGs than the 100-pg input replicates; **C)** Shared DEGs between the three input groups showing more DEGs that are unique than shared; **D)** Unsupervised analysis of CD5+ and CD5- samples by total RNA input amount. PCA reveals sample replicates separated by biological groupings at the 1,000- and the 100-pg input level but not at the 10-pg level.

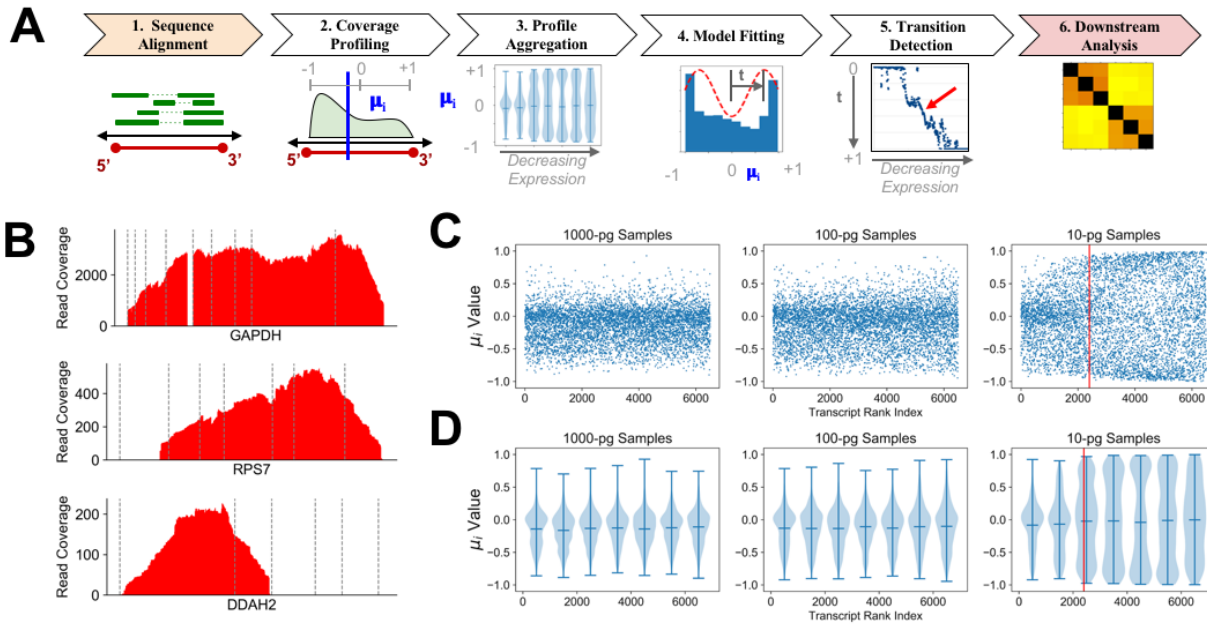


Figure 2

Figure 2. CLEAR Workflow: bin-based coverage analysis by transcript expression. A) Data analysis workflow using CLEAR to preprocess lcrRNA-seq data. Step 1: Trimmed lcrRNA-seq reads are aligned to the reference genome using HISAT2; Step 2: μ_i , the mean of the positional distribution of aligned reads along each individual transcript, is determined; Step 3: Transcript positional means, μ_i , (y-axis) are ranked and then binned by the transcript read coverage (x-axis). When μ_i of a bin is ≈ 0 , the read distribution is symmetrical along the length of the transcript. When μ_i within a bin develops a bimodal distribution with a mode near +1 (TTS) and one near -1 (TSS), its values will deviate from 0; Step 4: All available transcripts, binned into groups of 250 are fitted to a bimodal distribution model. The emergence of a bimodal distribution identifies when aggregate μ_i start to deviate from a unimodal distribution around the center of the transcripts, indicated by a change in the fitting parameter t ; Step 5: When the model parameter t passes a value of 0.5 (red arrow), transcripts beyond that point are excluded by CLEAR for differential gene expression and other downstream analysis; Step 6: CLEAR transcripts used in downstream between-group analyses such as hierarchical clustering; **B)** lcrRNA-seq read coverage plots. Read coverage plot for GAPDH depicts a transcript with $\mu_i \sim 0$. RPS7 depicts a transcript close to the $t = 0.5$ transition. DDAH2 depicts a transcript deemed too noisy by CLEAR; **C)** CLEAR profiles for 10-, 100- and 1,000-pg input mass lcrRNA-seq data. The value of μ_i is plotted for the 7,000 highest expressed primary transcripts for three representative samples. The red line depicts $t = 0.5$; **D)** violin plots of the same data as shown in Figure 2c. The end marks indicate the window extrema and the middle bar indicates the mean.

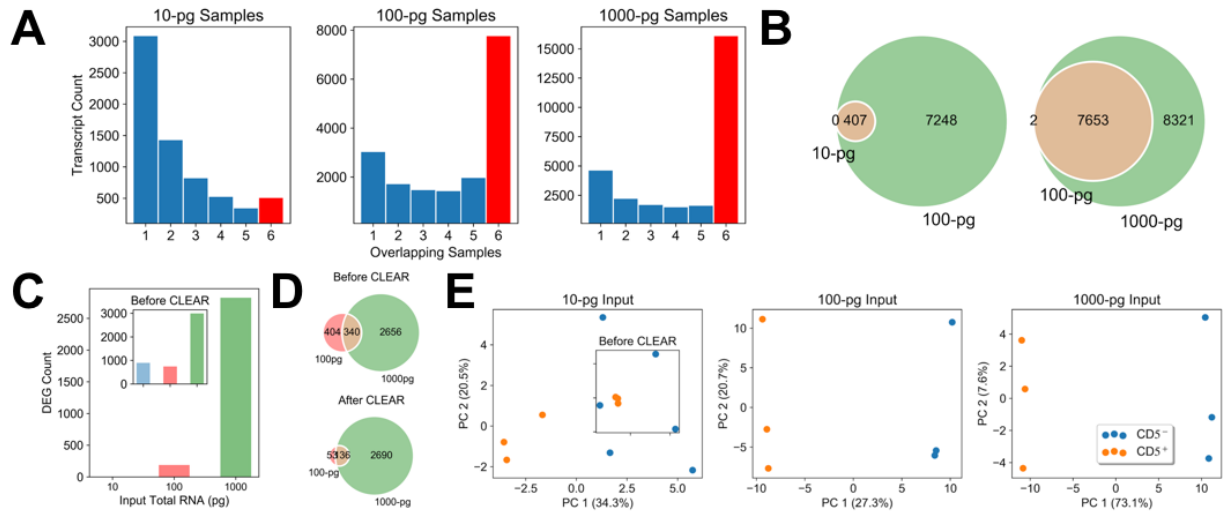


Figure 3

Figure 3. IcRNA-seq analyses between sample groups after application of CLEAR. **A)** CLEAR transcripts shared between samples of each input mass group. The red bars depict the number of CLEAR transcripts found in all 6 samples (replicates in both CD5+ and CD5- groups); **B) Left:** CLEAR transcripts overlap between 10-pg and 100-pg input mass samples; **Right:** CLEAR transcripts overlap between 100-pg and 1,000-pg input mass samples; **C)** DEG counts between CD5+ vs. CD5- cell types using only the shared CLEAR transcripts. The inset shows the data from Figure 1b without the application of CLEAR; **D)** Overlap of DEGs from the 100-pg and 1,000-pg inputs (inset repeats data from Figure 1c without CLEAR); **E)** PCA plots separating CD5+ and CD5- groups for all input masses using only CLEAR transcripts (inset repeats data from Figure 1d without CLEAR).

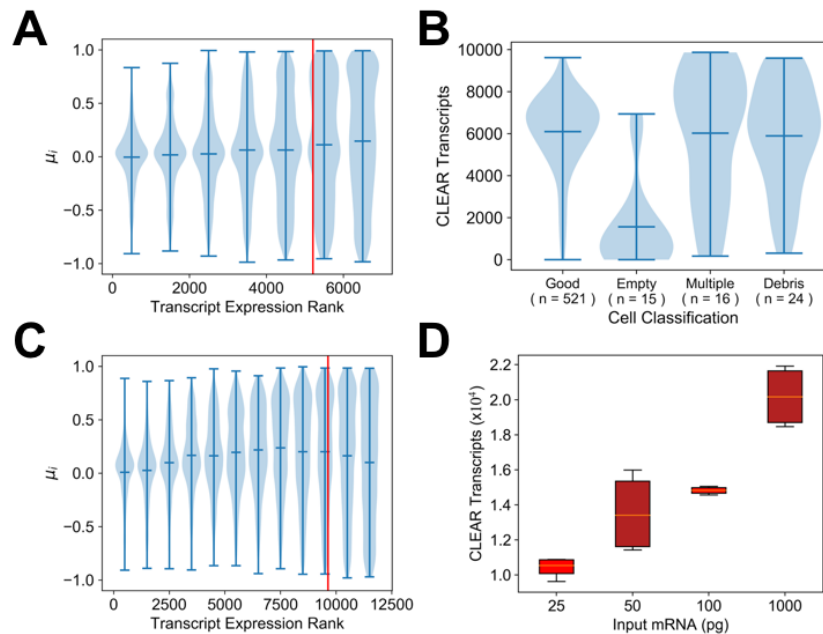


Figure 4

Figure 4. CLEAR discerns sample quality in publicly available datasets (Panels a and b: scRNA-seq, Ilicic et al. data (23); Panels c and d: lcrRNA-seq, Bhargava et al. (14)) **A)** CLEAR data preprocessing algorithm was applied to a scRNA-seq dataset derived from mouse embryonic stem cells

denoted as a ‘Good’ quality cell judging from microscopy inspection during the cell capturing step using the Fluidigm C1 IFC workflow. The resultant violin plots depict the gradual transition of $\mu_i \approx 0$ to $\mu_i \neq 0$ with the red line marking the point at which scRNA-seq transcripts are deemed unacceptable by the CLEAR criterion; **B**) The number of CLEAR transcripts from scRNA-seq data derived from mouse embryonic stem cells denoted as ‘Good’, ‘Empty’, ‘Multiple’ and ‘Debris’ are depicted as violin plots; **C**) CLEAR data preprocessing algorithm was applied to one of the lcrRNA-seq datasets (data from one of the two 25-pg mRNA input control samples) derived from polyA-selected mRNA extracted from control and Activin A-treated mouse embryonic stem cells. Once again, the resultant violin plots depict the gradual transition of $\mu_i \approx 0$ to $\mu_i \neq 0$ when transcripts are ranked and binned by their expression rate. The red line marks $t = 0.5$ after which scRNA-seq transcripts are deemed unacceptable by the CLEAR criterion; **D**) When we applied CLEAR to Bhargava et al. (14) serial dilution experiment data, we identified increasing amounts of CLEAR transcripts with increasing input mRNA amount. This is consistent with our observations in the CD5+/CD5- data shown in Figure 3c. Boxplots: orange line, mean CLEAR transcripts of two biological replicates per input mRNA amount; whiskers: displaying 1.5X the inter-quartile range (IQR) beyond the first and the third quartiles.

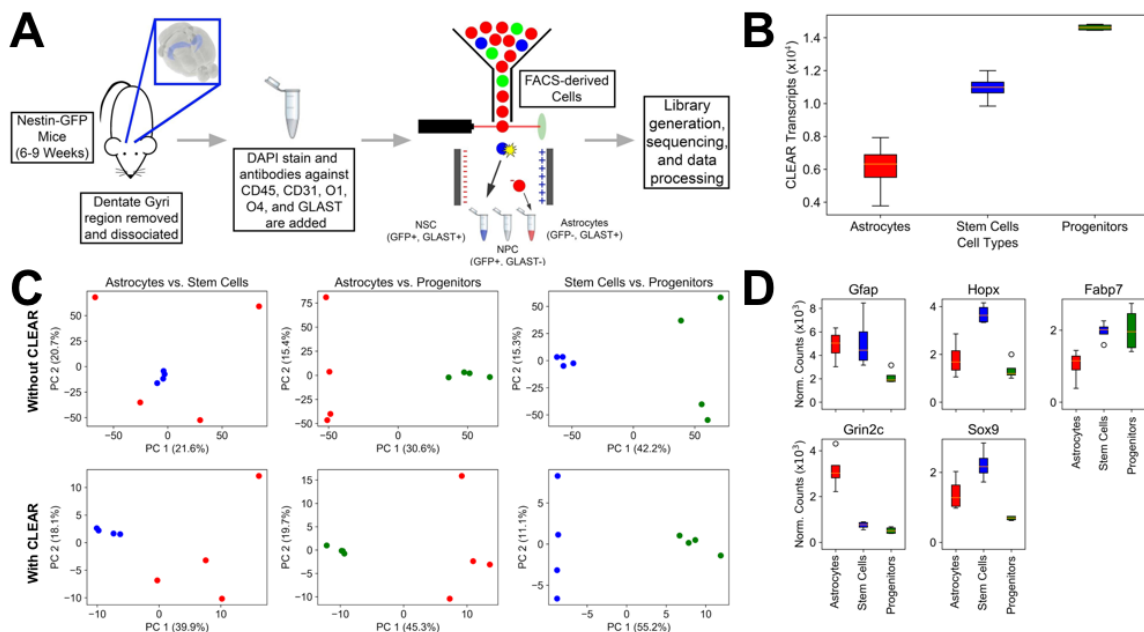


Figure 5

Figure 5. Application of CLEAR to a mouse neural lcrRNA-seq experiment: a proof of principle study. **A**) Schematic of cell isolation and preparation for sequencing. The dentate gyri of Nestin-GFP mice were microdissected and dissociated into a single cell suspension. Cells were labeled with fluorescently conjugated antibodies against markers for specific populations of cells present in the hippocampus. GFP+GLAST+ stem cells, GFP+GLAST- progenitor cells and GFP-GLAST+ astrocytes were isolated from live cells that were negative for microglial, oligodendroglial and endothelial markers. SMART-seq libraries were generated from these sorted cells; **B**) The means and ranges of CLEAR transcripts from each cell type (4 biological replicates per group). All groups are significantly different when compared using a t-test ($p < 0.01$); **C**) PCA analyses by murine neuronal cell types. *Top Panels:* PCA plots using all available transcripts; *Bottom Panels:* PCA plots using only CLEAR transcripts; **D**) Normalized DESeq2 transcript counts for 5 genes that pass CLEAR and are known to be differentially expressed in murine neural stem cells, progenitors and astrocytes are used to confirm the identity of the cell populations derived from the staining and FACS strategies used to enrich these three cell

populations. Boxplots: orange line, mean CLEAR transcripts for four biological replicates per neural cell type; whiskers: displaying 1.5X the inter-quartile range (IQR) beyond the first and the third quartiles; circles: outliers.

Gene	Astrocyte vs. Progenitor	Progenitor vs. Stem Cell	Astrocyte vs. Stem Cell
Gfap	N.S.	**	N.S.
Hopx	N.S.	****	**
Fabp7	**	N.S.	*
Grin2c	****	N.S.	***
Sox9	N.S.	****	N.S.
Neurod1	F.C.	F.C.	F.C.
Dcx	F.C.	F.C.	F.C.
Id4	F.C.	F.C.	F.C.
Pcna	F.C.	N.S.	F.C.
Mcm2	F.C.	F.C.	F.C.
Ascl1	F.C.	F.C.	F.C.
Eomes	F.C.	F.C.	F.C.
Nes	F.C.	F.C.	F.C.
Neurog2	F.C.	F.C.	F.C.

Table 1. Application of CLEAR and DESeq2 to murine DG cell type comparisons. Genes known to be differentially expressed in murine astrocytes, stem cells and progenitors. lcrRNA-seq data were preprocessed using CLEAR prior to between-group comparisons using DESeq2. Differential gene expression analysis evaluates the effectiveness of staining and FACS strategies in enriching these three cell types. The bisecting line indicates the border between transcripts which pass CLEAR in all samples and those that do not pass CLEAR in all samples. Each comparison was processed using DESeq2 and the significance of the comparison is given. *q*: FDR-corrected *p*-values; *N.S.* (Not Significant), *F.C.* (Failed CLEAR), * ($q \leq 0.05$), ** ($q \leq 0.01$), *** ($q \leq 0.001$), **** ($q \leq 0.0001$).

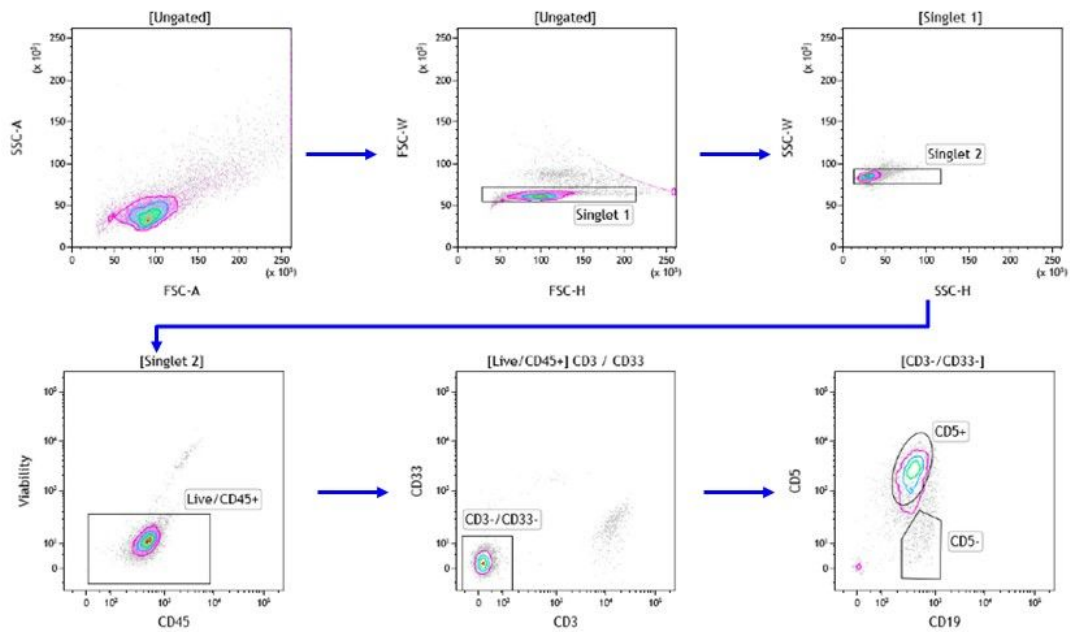


Figure S1. FACS parameter diagrams for the enrichment of CD5+ and CD5- cells from a CLL patient PBMC sample. FACS flow diagrams depicting the steps involved in the enrichment of CD5+ cells and CD5- cells from live CD45+, CD3-, CD33-, CD19+ cells.

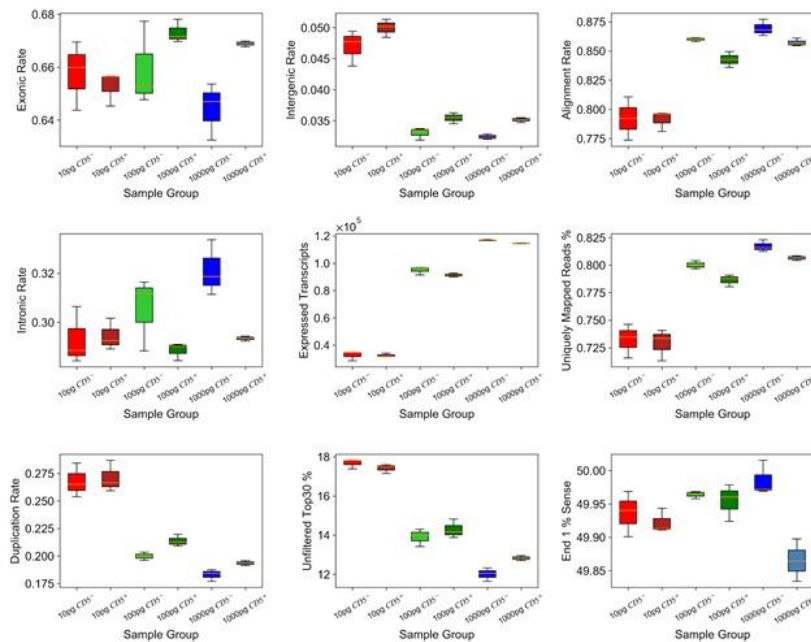


Figure S2. Selected quality control (QC) metrics.

Selected post-alignment RNA-seq QC metrics (shown on the y-axis) using a modified version of the QuaCRS (36) workflow highlighting the lcrRNA-seq composition- and quality changes with input mass in the CD5+ and CD5- data. Boxplots: yellow line, mean of the QC parameter; whiskers: displaying 1.5X IQR beyond the first and third quartiles.

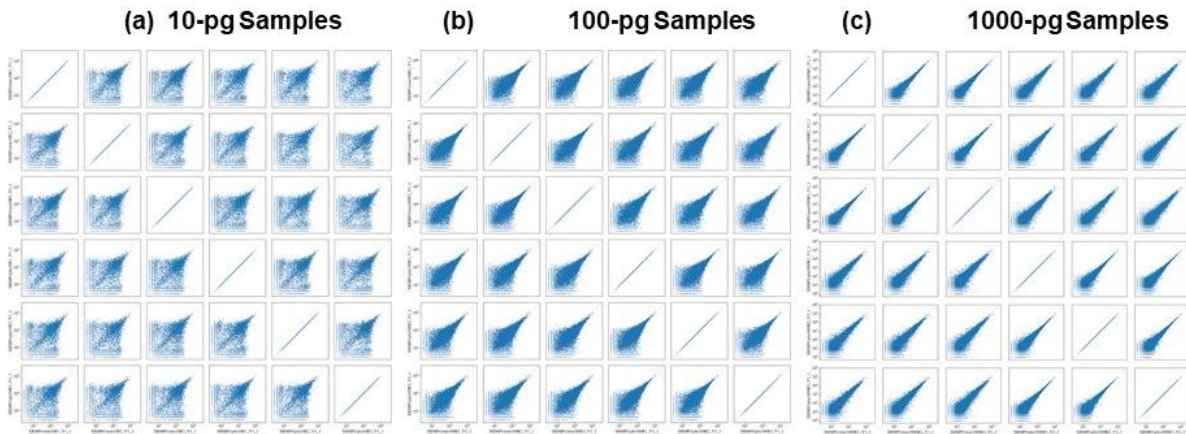


Figure S3. Scatterplots depicting all possible comparisons between the three CD5+ replicates and the three CD5- replicates at the three total RNA input masses for lcrRNA-seq library generation *before* CLEAR filtering. a) Input amount: 10-pg; b) Input amount: 100-pg; c) Input amount: 1,000-pg. Each panel represents one pair of comparisons and each dot represents the transcript amounts of the two samples being compared.

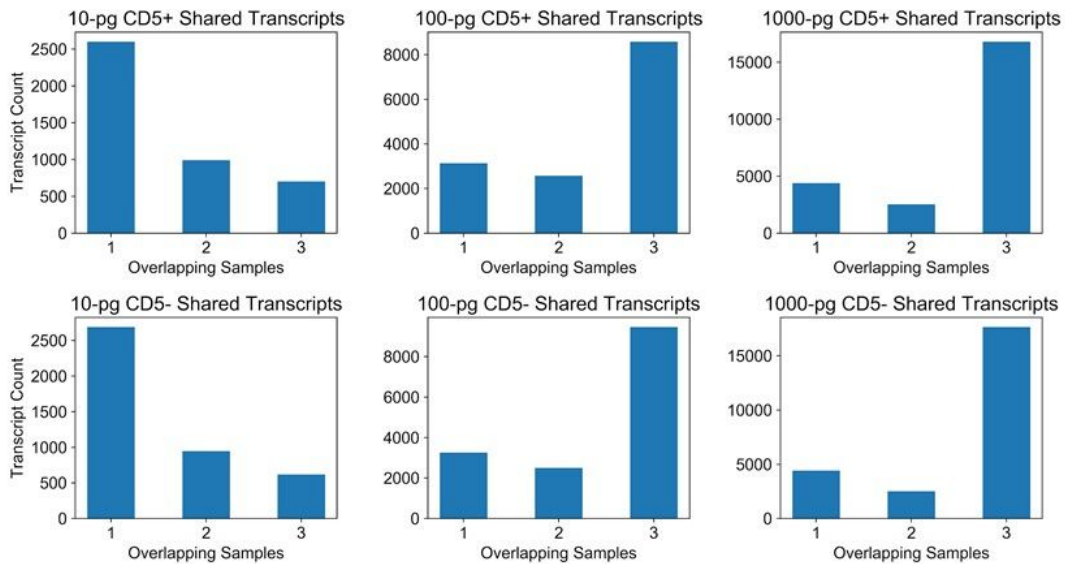


Figure S4. Shared CLEAR Transcripts in CD5+ and CD5- lcrRNA-seq data by input RNA mass. Similar to plots shown in Figure 3a with the exception that these plots are the shared CLEAR transcripts by cell types and by input total RNA mass.

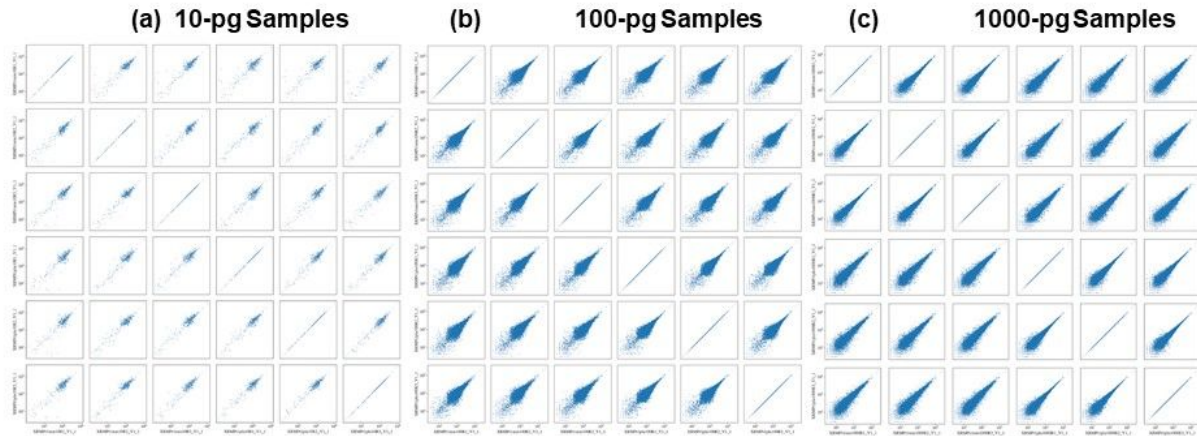


Figure S5. Scatterplots depicting all possible comparisons between the three CD5+ replicates and the three CD5- replicates at the three total RNA input mass for lcrRNA-seq library generation after CLEAR filtering. a) Input amount: 10-pg; b) Input amount: 100-pg; c) Input amount: 1,000-pg. Each panel represents one pair of comparisons and each dot represents the transcript amounts of the two samples being compared.

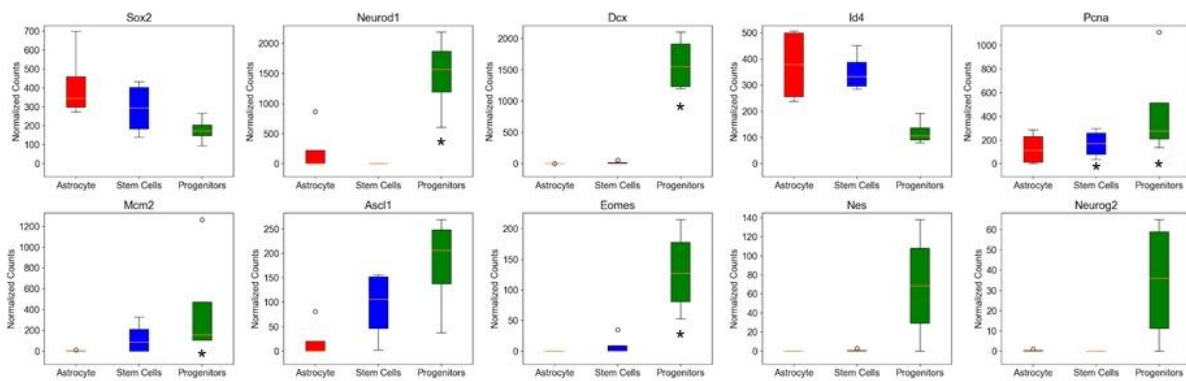


Figure S6. DESeq2 Normalized transcript counts for known murine neuronal cell surface markers that distinguish the three cell types. Plots depicting DESeq2 normalized transcript counts for selected cell surface markers (established in previous literature (47–51, 53) on these cell types) for murine astrocytes, progenitors, and stem cells ($n = 4$). Groups passing CLEAR are marked with an asterisk. Boxplots: yellow line, mean normalized DESeq2 counts for four biological replicates per neural cell type; whiskers: displaying 1.5X the IQR beyond the first and third quartiles; circles: outliers.